Predictive and dynamic signature for anti-angiogenics in combination with PD-1 inhibitor in soft-tissue sarcoma: correlative studies linked to the IMMUNOSARC trial

David S. Moura[1], Jesus M. Lopez-Marti[1], Iva Benesova[2], Carlos de Andrea[3], Davide di Lernia[1], Serena Lacerenza[4], Jose L. Mondaza-Hernandez[1], Marta Martin-Ruiz[1], Marta Ramirez-Calvo[5], Giovanni Grignani[6], Javier Martinez-Trufero[7], Andres Redondo[8], Claudia Valverde[9], Silvia Stacchiotti[10], Antonio Lopez-Pousa[11], José A. Lopez-Guerrero[5,12,13,], Antonio Gutierrez[14], Victor Encinas-Tobajas[15], Nadia Hindi[1,16,17], Dario Sangiolo[18], Jose A. Lopez-Martin[19], Zuzana Ozaniak Strizova[2], Javier Martin-Broto[1,16,17]

[1]Research health institute of Fundacion Jimenez Diaz (IIS/FJD; UAM), Madrid, Spain; [2] Department of Immunology, Second Faculty of Medicine, Charles University and University Hospital Motol, Prague, Czech Republic; [3]Department of pathology, Clinica Universidad de Navarra, Pamplona, Spain; [4]Institute of Biomedicine of Seville (IBiS; US, CSIC, HUVR), Seville, Spain; [5]Fundación Institute Valenciano of Oncology, Valencia, Spain; [6]Medical Oncology Unit, Città della Salute e della Scienza di Torino, Turin, Italy; [7]Medical oncology department, University hospital Miguel Servet, Zaragoza, Spain; [8]Medical oncology department, University hospital La Paz, Madrid, Spain; [9]Medical Oncology department, Vall d'Hebron University Hospital, Barcelona, Spain; [10]Medical Oncology department, Fondazione IRCCS Istituto Nazionale dei Tumori, Milan, Italy; [11]Medical Oncology department, Sant Pau Hospital, Barcelona, Spain; [12]Joint Cancer Research Unit IVO-CIPF, Valencia, Spain; [13]Department of Pathology, Medical School of the Catholic University of Valencia, Valencia, Spain; [14]Hematology department, University hospital Son Espases, Mallorca, Spain; [15]Radiology Department, University Hospital Virgen del Rocio, Sevilla, Spain;

[16]Medical Oncology Department, Fundacion Jimenez Diaz University Hospital; [17]University Hospital General de Villalba, Madrid, Spain; [18]Department of Oncology, University of Torino, Turin, Italy; [19]Medical Oncology department, University Hospital 12 de Octubre, Madrid, Spain

Current Address for J.A. Lopez-Martin: Precision Medicine, Atrys Health, Madrid, Spain.

Running title: Predictive signature for anti-PD-1-based therapies

Corresponding Author:

Javier Martin-Broto MD, PhD

Medical Oncologist, Fundacion Jimenez Diaz University Hospitals

Avda Reyes Catolicos 2, 28040 Madrid, Spain

28040, Madrid (Spain)

Phone: +34 629108979

jmartin@atbsarc.org

Conflict of interest disclosure: David S. Moura reports institutional research grants from PharmaMar, Eisai, Immix BioPharma, and Novartis outside the submitted work; travel support from PharmaMar, Eisai, Celgene, Bayer, and Pfizer, and personal fees from Tecnopharma, outside the submitted work. Andrés Redondo reports have received honoraria and provide advisory/consultancy services (MSD, AstraZeneca, GSK, PharmaMar, Boehringer Ingelheim, Pharma&), as well as research grant/funding to his institution (Eisai, PharmaMar, Roche), travel/accommodation/expenses (AstraZeneca, GSK, PharmaMar), and participation in a speaker's bureau (MSD, AstraZeneca, GSK, PharmaMar, Pharma&) outside the submitted work. Nadia Hindi reports grants,

personal fees, and non-financial support from PharmaMar, personal fees from Lilly and Tecnopharma, grants from Eisai, and Novartis, outside the submitted work and research funding for clinical studies (institutional) from PharmaMar, Eli Lilly and Company, AROG, Bayer, Eisai, Lixte, Karyopharm, Deciphera, GSK, Novartis, Blueprint, Nektar, Forma, Amgen and Daichii-Sankyo. Jose A. Lopez-Martin was a former employee at PharmaMar, SA. Javier Martin-Broto reports research grants from PharmaMar, Eisai, Immix BioPharma, and Novartis outside the submitted work; honoraria for advisory board participation and expert testimony from PharmaMar, Eli Lilly and Company, Bayer, GSK, Novartis, Boehringer Ingelheim, Amgen, Roche, Tecnofarma and Asofarma; and research funding for clinical studies (institutional) from PharmaMar, Eli Lilly and Company, BMS, Pfizer, AROG, Bayer, Eisai, Lixte, Karyopharm, Deciphera, GSK, Celgene, Novartis, Blueprint, Adaptinmune, Nektar, Forma, Amgen, Daichii-Sankyo, Rain Therapeutics, INHIBRX, Ayala Pharmaceuticals, Philogen, Cebiotex, PTC Therapeutics, Inc. and SpringWorks therapeutics. The remaining authors declare no conflicts of interest.

STATEMENT OF TRANSLATIONAL RELEVANCE

The predictive molecular-based signature described in this study can help us in the identification of patients with soft-tissue sarcoma, responding to PD1 immune checkpoint inhibitors in combination with tyrosine kinase inhibitors. This predictive signature is a potential alternative to the presence of tertiary lymphoid structures, as a predictive biomarker for PD-1 inhibitors treatment, mainly in cases in which a core biopsy could overlook tertiary lymphoid structures presence, due to its peripheral predominant distribution. The molecular dynamic alterations identified in response to treatment can also help us to understand how anti-angiogenics inflame sarcoma milieu and the biology behind anti-PD-1 activity. These dynamic alterations in response to treatment may be helpful to optimize patient treatment, through the design of novel clinical trials for soft-tissue sarcoma patients.

ABSTRACT

Purpose: IMMUNOSARC trial combined an anti-angiogenic agent (sunitinib) with a PD-1 inhibitor (nivolumab) in advanced sarcomas. Here we present the first correlative studies of the STS cohort enrolled in this trial.

Experimental design: Formalin-fixed paraffin-embedded (FFPE) and peripheral blood samples were collected at baseline and week 13. FFPE were used for transcriptomics and multiplex immunofluorescence, while peripheral blood samples were used for multiplexed immunoassays. Flow cytometry and Luminex assays were performed to validate translational findings in tumor-isolated cells and peripheral blood mononuclear cells derived from patients.

Results: The density of intratumoral CD8+ T cells, measured by multiplexed immuno-phenotyping, was significantly increased after treatment. This augment was accompanied by the dynamic significant increase in gene expression of CD86, CHI3L1, CXCL10, CXCL9, LAG3, and VCAM1, and the decrease in the expression levels of NR4A1. In peripheral blood, 12 proteins were significantly modulated by treatment at W13. A score integrating the dynamic expression of the 7 genes and the 12 soluble factors separated two groups with distinct progression-free survival (PFS): 4.1 months (95% CI 3.5-NR) vs 17 months (95% CI 12.0 – NR), p=0.014. This molecular score was predictive of PFS when applied to the normalized data determined in the baseline samples.

Conclusions: Treatment with sunitinib and nivolumab inflamed the sarcoma microenvironment, increasing CD8+ T cell density and the expression of several genes/

proteins with relevance in the response to PD-1 inhibitors. A molecular signature identified two groups of patients with distinct PFS for the combination of anti-angiogenics plus PD-1 inhibitor.

INTRODUCTION

Sarcomas, a group of rare malignancies arising from connective tissues, constitute a therapeutically challenging family of tumors partially owing to their inherent heterogeneity and rarity. Immunomodulation inhibiting the programmed cell death protein 1 (PD-1)/programmed cell death protein 1 ligand (PDL-1) axis has recently emerged as a crucial backbone in several tumors, such as melanoma or non-small cell lung cancer. In the sarcoma scenario, novel strategies to harness the immune system against these tumors have been attempted.(1) Usually, the sarcoma tumor microenvironment is less responsive to anti-PD-1/anti-PD-L1 compounds. Thus, innovative approaches are being tested to induce an inflamed microenvironment that can potentially be translated into highly responsive tumors.(2)

Clinical trials investigating the efficacy of PD-1 inhibitors in sarcomas have shown encouraging results for specific cancer subtypes.(3-5) Noteworthy that studies testing the combination of anti-PD-1 inhibitors with other immune checkpoint inhibitors (ICIs)(5) or with anti-angiogenics(3) showed superior activity, with a few exceptions such as in alveolar soft-pat sarcoma (ASPS)(6), by indirect comparisons with PD-1 inhibitors in monotherapy, suggesting that strategies to inflame the sarcoma tumor immune microenvironment (TIME) are key to improving the activity of anti-PD-1.

Among these clinical trials, IMMUNOSARC (ClinicalTrials.gov ID: NCT03277924) is a study that tested the combination of an anti-angiogenic agent (sunitinib) with an anti-PD-1 (nivolumab) in selected types of soft-tissue sarcoma (STS) and bone tumors, with

the idea of using anti-angiogenic treatment as a way to inflame TIME. Tumor angiogenesis is related to the suppression of T cells and prevents immune adaptive responses, through complex mechanisms that are potentially linked to tissue homeostasis. Numerous hematopoietic cells, such as myeloid-derived suppressor cells, dendritic cells, and macrophages, can secrete mediators, such as VEGF-A, which have a well-known function in both angiogenesis and immunosuppression.(7) T cells exposed to hypoxia and intra-tumoral T cells within the tumors express VEGF-A.(8) Among these T cells, $CD4^+$ regulatory T cells seem to contribute to angiogenesis more clearly in an adequate context.(9) Thus, anti-angiogenic treatment would promote TIME inflammation, by blocking immunosuppression, activating immune adaptive response, and improving the activity of PD-1 inhibitors.

In our IMMUNOSARC STS cohort, the combination of anti-PD-1 and sunitinib was safe and showed activity at least in some histologies among those who were investigated, with an overall 6-month progression-free survival (PFS) of 48% and an mPFS of 5.6 months as an option for second-line treatment in progressing patients. The clinical benefit was 85%, however, the RECIST overall response rate (ORR) was only 21%(3), suggesting that it is necessary to identify prognostic and/or predictive biomarkers and better understand the biological mechanisms modulated by ICI, particularly by inhibiting the PD-1/PD-L1 axis to improve patient selection for this type of treatment and design better clinical trials.

In general, the efficacy of PD-1 inhibition in sarcomas is influenced by the cellular composition and the production of various molecules in the TIME. Among the most prominent molecules is PD-L1 and the complex interplay of various soluble molecules including cytokines, chemokines, and growth factors.(10)

This correlative translational study aimed to profile the molecular changes over time in various components, such as tumor microenvironment cellularity, and cytokines. These changes describe the biological and cellular processes, modulated by the combination treatment of anti-angiogenic agents and PD-1 inhibitors, in patients enrolled in the prospective clinical trial IMMUNOSARC, where sunitinib and nivolumab are administered in combination.

MATERIALS AND METHODS

Patients and samples

Patients with selected STS histologies were treated with sunitinib and nivolumab in the IMMUNOSARC clinical trial (ClinicalTrials.gov ID: NCT03277924) and included in these correlative studies. All the patients were in progression before enrolment in the clinical trial. STS histologies included alveolar soft-part sarcoma (ASPS), angiosarcoma, clear cell sarcoma, epithelioid sarcoma, extraskeletal myxoid chondrosarcoma (EMC), hemangioendothelioma, solitary fibrous tumor (SFT), synovial sarcoma, and undifferentiated pleomorphic sarcoma (UPS). Trial information, including the treatment scheme and inclusion/ exclusion criteria, has been previously published.(3) Formalin-fixed paraffin-embedded (FFPE) tumor samples derived from biopsies taken at baseline (within the 28 days previous treatment initiation) and at week 13 (cycle 3, day 1) were collected, whereas peripheral blood samples were obtained at baseline (within the 72h previous to treatment initiation) and at week 13 (second radiologic evaluation, beginning of the third cycle of treatment) (Supplementary Figure S1). The study was approved by the Institutional Review Board of the University Hospitals Virgen Macarena–Virgen del Rocío Ethics Committee and was performed according to national regulations and following the Declaration of Helsinki. The patients signed the written informed consent to participate in the study.

HTG Oncology Biomarker panel

Targeted RNA-Seq was used to evaluate gene expression levels in pre- (baseline; N=64) and post-treatment (week 13; N=34) FFPE samples (Supplementary Figure S1), using the HTG Oncology Biomarker Panel (OBP), according to manufacturers' instructions and as previously reported (*ad hoc* study).(3,11)

Measurement of serum cytokine level with Immune Monitoring 65-Plex Human ProcartaPlex™ Panel

The concentration of 65 soluble factors including cytokines, chemokines, and growth factors, were analyzed using the Human Immune Monitoring 65-Plex ProcartaPlex Panel (Invitrogen™, Thermo Fisher Scientific, Waltham, MA, USA), in 25 µL of plasma sample for each patient (*ad hoc* study). Briefly, antibody-coated beads against the different cytokines and soluble factors were incubated for 2 hours with plasma samples in 96-well plates. A biotinylated detection Antibody Mix, followed by Streptavidin-PE (SA-PE) was used, according to the manufacturer's protocol. All measurements were performed in duplicate. The standard curve was drawn using standards of known concentrations from the kit. Mean fluorescence intensity (MFI) and concentration data have been obtained using the Bio-Plex 200 System (Bio-Rad; Hercules, CA, USA) instrument, and analyzed through the ProcartaPlex™ Analyst Software, according to the manufacturer's instructions. Plasma collected at baseline (n=59) and week 13 (n=35) were used for these determinations (Supplementary Figure S1).

Multiplexed Immunofluorescence Staining and Tissue Imaging

Using a previously validated and standardized multiplexed immunofluorescence protocol and whole tumor tissue sections, we simultaneously measured the expression

of CD20 (IgG2α, mouse monoclonal, clone: L26, ready-to-use; Agilent), CD3 (IgG, rabbit polyclonal, ready-to-use; Agilent), CD8 (mouse monoclonal, clone: C8/144B, ready-to-use; Agilent), CD68 (mouse monoclonal, clone: PG-M1, ready-to-use; Agilent), CD66b (mouse monoclonal, clone: 80H3, dilution: 1:200; LS-Bio), CD138 (mouse monoclonal, clone: MI15, dilution: 1:100; Agilent), and DAPI(12) – *post hoc* study. The validation workflow consisted of optimizing each marker in single protocols. They were then integrated into a multiplexed immunofluorescence protocol. Each single antibody was optimized individually for its optimal conditions and position in the sequence of multiplex staining. Tonsil tissue was used as positive controls to establish the concentrations of the primary antibodies. The multiplexed immunofluorescence assay was performed on a fully automated Leica Bond Rx autostainer. In brief, tissue sections were deparaffinized and subjected to sequential rounds of antibody staining. Antigen retrieval was performed using BOND Epitope Retrieval solution 1 (ER1; Cat. AR9961). Secondary antibody incubation was carried out with a mix of HRP-conjugated anti-mouse/rabbit secondary antibodies and tyramide signal amplification visualization (both included in the Opal 7-Color Automation IHC Kit; Cat# NEL871001; Akoya Bioscience) with fluorophores Opal 520, 540, 570, 620, 650, and 690 (dilution for all Opals: 1:100 in 1x amplification buffer, all included in the Opal IHC Detection Kit; Akoya Bioscience)as described previously.(12,13) Nuclei were then counterstained with spectral DAPI (Akoya Bioscience). Sections were then mounted with Faramount Aqueous Mounting Medium (Dako).

Multiplexed immunofluorescence slides were scanned on a Vectra-Polaris Automated Quantitative Pathology Imaging System (Akoya Biosciences). Spectral unmixing was performed using inForm software (version 2.4.8, Akoya Biosciences) as described.(14) Cells were phenotyped using the open-source digital pathology software QuPath version

0.2.3 (University of Edinburgh, Edinburgh, UK; https://qupath.github.io), as described.(15) Cells were segmented based on nuclear detection using the StarDist 2D algorithm. A random trees algorithm classifier was trained for each cell marker. Cells were then subclassified as $CD68^+$, $CD3^+$, $CD8^+$, $CD66b^+$, $CD20^+$, and $CD138^+$ cells. $CD4^+$ T-cells were defined as $CD3^+$ $CD8^-$. Cells negative for these markers were defined as "other cell types". Measurements were calculated as cell densities (cells/mm^2). Tertiary lymphoid structures (TLS) were defined by dense aggregates of $CD3^+$/ $CD8^+$/ $CD20^+$. TLS were determined as total counts in all analyzed tissue sections for each patient. Tumor biopsies collected at baseline (n=42) and week 13 (n=22) were used for the multiplexed immunofluorescence assay (Supplementary Figure S1).

Bioinformatics and statistical analysis

Data analysis was conducted in R (RRID:SCR_001905) using the Bioconductor (RRID:SCR_006442) and plotting packages (RRID:SCR_021139 and RRID:SCR_014601). The raw gene counts were normalized using DESeq2 (RRID:SCR_015687), with the batch effect employed for normalization. Subsequently, genes were filtered based on a p-adjusted threshold of 5%. Differentially expressed genes (DEGs) were identified between the baseline samples and after treatment (week 13). A total of 68 samples, comprising 34 baseline and 34 week 13 samples were used for this analysis.

The Wilcoxon paired test R package version 1.1.1 (https://doi.org/10.32614/CRAN.package.PairedData) was used to identify the soluble factors and cell densities differentially expressed between baseline and week 13 samples and to correlate PFS with the dynamic alteration of soluble factors protein expression and cell densities. Histology was not included as a variable in the bioinformatics

analysis, since we did not observe any relation between indolent histologies or those histologies more sensitive to antiangiogenics and patient outcome in the clinical study, as previously published.(3)

To estimate the absolute abundance of immune cell infiltration in both the basal and week 13 datasets, we used CIBERSORTx (RRID:SCR_016955).(16) The normalized gene counts from dynamic datasets (68x2559) were estimated into immune cell absolute abundances using the predefined LM22 matrix using B-mode batch correction. The abundance of certain immune cell types was performed considering only the genes in common between the HTG OBP panel and the LM22 matrix (164 out of 547). To validate the performance of the LM22-HTG resulting cell type gene signatures, granulator (RRID:SCR_022158.) benchmark functionality was used with a set of whole blood RNASeq mixtures (GSE127813) with available known ground truth for certain cell types (flow cytometry).(17) A Pearson correlated value of 0.75 (SVR algorithm)(17), between estimated abundance and ground truth values, was established as a threshold to keep the highest correlated cell types. The granulator benchmark validates the use of the HTG panel for T.CD8 (T.cells.CD8 and T.cells.gamma.delta), T.CD4 cells (T.cells.CD4.memory.activated + T.cells.CD4.memory.resting + T.cells.CD4.naive + T.cells.follicular.helper), Monocytes and B.Cells (B.cells.memory + B.cells.naive). For this study, we only consider CIBERSORTx results of these cell types.

Time-to-event variables (PFS) were measured from the date of therapy onset and were estimated according to the Kaplan-Meier method. The comparisons between the variables of interest were performed by the log-rank test. The Cox proportional hazard regression model was applied to the multivariate analysis with the variables that appeared to be significant in the univariate analysis. The validity of the proportional

hazard assumption was verified by adding a time-dependent variable to each model to confirm that HR for each covariate did not increase or decrease over time. Student's t-test was used to detect statistically significant differences between treatment groups in the pre-clinical experiments. All p-values reported were 2-sided, and statistical significance was defined at $p < 0.05$. The analyses were carried out in SPSS version 25.0 (IBM; Armonk, NY, USA; RRID:SCR_002865).

Construction of molecular scores

Molecular scores were built considering the dynamic levels of genes and/ or soluble factors differently expressed between the baseline and week 13. The score was first obtained by calculating the cut-off points with the MAXSTAT R package version 0.7-25 (https://doi.org/10.32614/CRAN.package.maxstat), and then by discretizing the values between high and low for each scorer (gene or cytokine). Then, the discreet values were used to calculate a coefficient with Cox proportional hazards regressions, to determine whether it had a negative or positive value, concerning the "low" value (reference). If the coefficient sign was negative or positive, a value of 1 (good prognosis) or 0 (poor prognosis), respectively, was assigned. After processing all markers (soluble factors and DEG) the 1/0 values, obtained in the previous process, were assigned to each marker to calculate the final score by sample. The final scores ranged from 0 to 7 for genes, 0 to 12 for soluble factors, and 0 to 19 for genes and soluble factors. Finally, MAXSTAT was used to calculate the optimal cut-off for each score, to discreet the study population in the two groups, and to create a Kaplan survival curve (RRID:SCR_021137 and RRID:SCR_021094).

Pre-clinical studies

Isolation of PBMC

Peripheral blood from five leiomyosarcoma patients was collected into EDTA tubes. Afterward, the blood was mixed 1:1 with phosphate-buffered saline (PBS) supplemented with 2 mM EDTA. This mixed suspension was transferred into a SepMATE™ PBMC isolation tube (STEMCELL Technologies, Vancouver, Canada) that contained 15 ml of Ficoll-Paque PLUS (Cytiva Sweden AB, Uppsala, Sweden). The tube was centrifuged at 1200 g for 10 min at room temperature (RT). Afterward, the upper layer was quickly poured into a new tube and washed twice with PBS. The cells were cryopreserved until further use.

Isolation of cells from tumor tissue

Five surgically resected leiomyosarcomas were obtained from the Third Department of Surgery, First Faculty of Medicine, Charles University and University Hospital Motol, Prague, Czech Republic. Firstly, the tumor tissue was transferred into a gentleMACS™ C tube (Miltenyi Biotec, Bergisch Gladbach, Germany) and cut into small pieces with scissors, afterward, RPMI 1640 medium (Thermo Fisher Scientific, Waltham, MA) supplemented with 1 mg/ml of collagenase I (Roche, Basel, Switzerland) and 0.05 mg/ml DNase I (Roche) was added. The tissue was further dissociated using the gentleMACS™ dissociator (Miltenyi Biotec) at program h_tumor_01. Subsequently, the suspension was digested for 30 min at 37 °C on a shaker. Next, the mixture was again dissociated by gentleMACS™ at program h_tumor_01 and passed through a 100 µm nylon cell strainer (Corning, New York, USA) into a new tube. The cell suspension was washed by PBS, and subsequently, the red blood cells were lysed for 10 min at RT and centrifuged at 300 g, 5 min, RT. The cells were cryopreserved until further use.

Selective T-cell stimulation, therapeutic blockade, and flow cytometry

The isolated PBMC and tumor-isolated cells (N=10) were used for the *in vitro* testing of a PD-1 inhibitor (Selleck Chemicals, Houston, USA). The PBMC were divided into four groups; unstimulated cells, unstimulated cells + vehicle control (0.2% DMSO), anti-CD3/CD28 (0.5 mg/ml, Thermo Fisher Scientific, Waltham, MA, USA) stimulated cells, and anti-CD3/CD28 stimulated cells + PD-1 inhibitor (2 µg/ml). Tumor-isolated cells were divided only into three groups since the number of cells was low and not sufficient for four treatment groups. Thus, and since we did not observe any effect of DMSO in PBMC, we excluded the unstimulated DMSO-treated group from the experiment. The 250 000 PBMC or 200 000 tumor-isolated cells were cultivated for 24 hours at 37 °C, 5% CO_2 in 250 µl of culture medium (RPMI 1640 supplemented with 10% heat-inactivated fetal bovine serum (Cytiva), 100 U/ml penicillin-streptomycin, and 2mM GlutaMax (Thermo Scientific)). Afterward, the samples were centrifuged (300 g, 5 min, RT) and the supernatant was collected for the analysis by multiplex Luminex cytokine bead-based assay and the cells were stained by flow cytometry to investigate the frequencies of T cell subsets with the main focus on inhibitory molecules such as PD-1 and LAG-3. Briefly, the cells were firstly stained by Zombie NIR™ fixable viability kit (Biolegend, San Diego, California, USA) for 20 min, at RT in the dark. Then, the cells were washed in PBS, centrifuged and fluorescently-labeled monoclonal antibodies were added; CD3 – PerCP/Cy5.5 (RRID:AB_10640736; Biolegend), LAG-3-PE-Cy7 (RRID:AB_2629753; Biolegend), PD-1 - BV421 (RRID:AB_10960742; Biolegend), CD4 PE-Dylight 594 (RRID: AB_3492078; Exbio, Vestec, Czech Republic), CD8 – FITC, (RRID:AB_10735944 Exbio), and incubated for 20 min, 4 °C, in the dark. The cells were washed in PBS and analyzed by BD LSR Fortessa cytometer. Subsequent analyses were performed in FlowJo

(RRID:SCR_008520; BD Bioscience, v10.10). Fluorescence minus one control was included to set proper gates.

Multiplex Luminex cytokine bead-based assay

The custom human XL cytokine 16-plex kit (Lot number: 1645358; Bio-techne, Minneapolis, MN, USA) was utilized according to manufacturer protocol. The kit included following cytokines: TNFα, IFNγ, Granzyme B, IL-2, IL-15, TRAIL, CCL2, CXCL10, MIP-1α, IL-8, IL-17, TRAIL, MIP-1β, IL-10, PD-L1, VEGF and CCL5. Briefly, 25 µl of supernatant was diluted 1:1 in the calibration diluent. Subsequently, a microparticle cocktail was added and the whole suspension was incubated on a shaker for 24 hrs at 4 °C. Subsequently, the samples were washed three times and the biotin-antibody cocktail was incubated for 1 hour at RT on the shaker. After the next washing, streptavidin-PE was incubated for 30 min at RT on the shaker. The samples were washed again and analyzed by the Luminex 200 system and Bellisa software (Merck Millipore, Burlington, MA, USA).

Data Availability Statement

The data generated in this study are not publicly available since the informed consent signed by the patients did not include this option. However, the data are available upon reasonable request from the corresponding author.

RESULTS

Patients' demographics

A total of 65 STS patients, enrolled within the multicenter, single-arm phase Ib/II clinical trial, testing the combination of sunitinib, and nivolumab were eligible for this correlative study.(3) The median age was 40 years (range, 20–78 years). Thirty-nine

(60%) and 26 (40%) patients were male and female, respectively. A total of 94% (n=61) of the patients had metastatic disease at the time of treatment initiation, while 6% (n=4) had unresectable locally advanced disease. The ECOG status at baseline was 0 or 1 in 31 (48%) and 34 (52%) patients, respectively. According to the central pathology review, the most frequent histological types were clear cell sarcoma (17%; n=11), synovial sarcoma (17%; n=11), and undifferentiated pleomorphic sarcoma (UPS; 15%; n=10). The complete patient demographics are depicted in Table 1. Tumor biopsies were collected at baseline (n=64) and week 13, after the first day of cycle 3 (n=34/64, 53%). Peripheral blood samples were collected at baseline (n=59) and week 13 (n=35/59, 59%) (Supplementary Figure S1).

Spatial immunophenotyping analysis

The immunomodulatory effect of the treatment on immune cell densities was assessed by comparing the baseline (n=42) and week 13 (n=22) FFPE tumor blocks. In paired samples, CD3 (p=0.006) and CD8 (p=0.011) cell densities were significantly increased at week 13, suggesting that $CD8^+$ T cells were augmented by treatment (Figure 1A and 1B). No significant changes in cell densities were detected for CD4, CD20, CD66b, CD68, or CD138 (Figure 1C-1G). Notably, patients with a better PFS (MAXSTAT cut-off of 9.4 months) had a significant increase in $CD3^+$ cell density after treatment, while this increase was not detected in patients with a lower PFS (Supplementary Figure S2A). Changes in the cell densities of the other cytologic markers did not correlate with PFS; however, patients with better PFS showed a trend for increased $CD8^+$ density at week 13 (p=0.084) (Supplementary Figure S2B-S2G).

Immune cell densities were estimated in FFPE tumor samples freshly collected at baseline (Figure 1), (N=42) and correlated with clinical outcomes (PFS and overall survival) in a univariate analysis. Higher $CD8^+$ T cell density (>12.30 cells/ mm^2) was

associated with better PFS [2.1 months (95% CI 0-4.7) vs. 4 months (95% CI 0-8.7), p=0.040], whereas CD3, CD4, CD20, CD66b, CD68, and CD138 cell densities did not show any significant association with clinical outcomes (Supplementary Table S1).

Tertiary lymphoid structures (TLSs) were identified in 11 of 42 evaluable patients, considering both the baseline and week 13 tumor blocks (64 samples in total). The presence of TLS, defined by dense aggregates of $CD3^+$/ $CD8^+$/ $CD20^+$ B cells, showed a trend for better PFS compared to cases without detectable TLSs: 11.9 months (95% CI 3.5-20.3) vs. 3.3 (95% CI 2.4-4.3), p=0.059.

Deconvolution analysis of gene expression

Normalized gene expression levels, determined in FFPE samples, were used for deconvolution analysis with CIBERSORTx to accurately estimate the dynamic proportion of immune cell-infiltrating tumors, between baseline and after treatment, and to determine if these changes had prognostic value for PFS. In the CIBERSORTx data, no significant changes were observed in the abundance of B Cells between baseline and after treatment (Figure 2A), nor did the abundance of B cells correlate with patient survival (Figure 2B). Similar results were observed for CD4+ T cells (Figures 2C and 2D), however, we observed that treatment induced an increase in $CD8^+$ T Cells at week 13 (p=0.005) (Figure 2E), which was in line with the increase in CD8 density observed at the protein level by multiplexed immunohistochemistry. Of note, patients with a better PFS (MAXSTAT cut-off of 5.6 months) had a significant increase, at week 13, in the abundance of $CD8^+$ cells (p<0.001) – Figure 2F. The abundance of monocytes was not altered due to treatment (Figure 2G), nor did the abundance of this immune cell type correlate with patient survival (Figure 2H).

Differential gene expression

Differential gene expression was determined in a subset of baseline and week 13 paired samples (N=34). Seven genes were significantly and differentially expressed after treatment: *CD86* (log2FC=0.698; p=0.042), *CHI3L1* (log2FC=1.185; p=0.024), *CXCL10* (log2FC=1.414; p=0.012), *CXCL9* (log2FC=1.836; p=0.018), *LAG3* (log2FC=087; p=0.024), *NR4A1* (log2FC=-1.072; p=0.024), and *VCAM1* (log2FC=0.994; p=0.022). The expression of *NR4A1* decreased after treatment, whereas the expression of the other six genes increased at week 13 (Supplementary Table S2). In the univariate analysis, a greater increase in the dynamic expression (Δ) of *CD86* [3.7 months (95% CI 3-4.4) vs. 11.3 months (95% CI 7.4-15.1), p=0.045], *CXCL10* [4.1 months (95% CI 3-5.3) vs. 11.9 months (95% CI 7.6-16.2), p=0.016], *LAG3* [3.5 months (95% CI 3.1-3.9) vs. 7.5 months (0-14.9), p=0.008], and *VCAM* [4 months (95% CI 2.6-5.4) vs. 13.5 months (95% CI 9.7-17.3), p=0.031] was significantly associated with longer PFS. Concerning *CHI3L1*, the dynamic increase in the expression level of this gene was strongly correlated with a shorter PFS [7 months (95% CI 0-14.3) vs. 3.7 months (95% CI 3.4-3.9), p=0.030]. The dynamic differences in the expression levels of *CXCL9* or *NR4A1* did not show any correlation with survival (Supplementary Table S3). The MAXSTAT cut-offs for differential gene expression used for univariate analysis are shown in Supplementary Table S4. In the multivariate analysis, considering the genes with significant prognostic value in the univariate analysis, only the higher dynamic increase in the expression of *CXCL10* and *LAG3* were independent factors for mPFS: HR 2.7 (95% CI: 1.2-6.3); p=0.019 and HR 3.9 (95% CI: 1.3-11.2); p =0.013, respectively. The overexpression of either *CXCL10* or *LAG3* at week 13 was associated with better mPFS.

Multiplexed immunoassays in peripheral blood plasma

Differential soluble protein expression was determined in samples collected at baseline and week 13 (n=35). Twelve soluble proteins were differentially expressed and reached statistical significance in the paired samples: CXCL13 (BLC; p<0.001), CD30 (p=0.018), eotaxin (p<0.001), CXCL11 (I-TAC; p=0.005), IL-2R (p<0.001), IL-4 (p<0.001), IL-8 (p=0.008), CXCL10 (IP-10; p<0.001), CCL2 (MCP-1; p<0.001), CCL8 (MCP-2; p=0.007), CCL22 (MDC; p=0.007), and VEGF-A (p=0.030) (Supplementary Figure S3). Except for CD30, the dynamic alteration in the protein expression levels of these soluble factors had an impact on PFS (Figure 3). More precisely, patients with a better PFS (MAXSTAT cut-off of 7.2 months) had a significant increase, at week 13, in the expression levels of CXCL13, IL-2R, CXCL11, CCL8, IL-4, Eotaxin, IL-8, CXCL10, CCL2, and VEGF-A, and a significant decrease in the expression levels of MDC. Of note, the significant difference observed in the expression of CXCL10 at the protein level in plasma between baseline and week 13, was also determined at the gene level by transcriptomics in the tumor. The TLS marker CXCL13 was also significantly overexpressed at week 13 and was correlated with better PFS. Additionally, we detected other soluble factors with an impact on PFS, despite the lack of significance in the dynamic alteration of their expression levels. Patients with a better PFS (MAXSTAT cut-off of 7.2 months) showed a significant increase, at week 13, in the expression levels of APRIL, ENA-78, SCF, and TNF-RII (Supplementary Figure S4).

Molecular scores

Molecular scores were built considering the 7 significant DEGs and/or the 12 soluble factors differentially expressed between baseline and week 13. The prognostic and/or predictive gene-based score divided our population into two groups with different PFS: patients with a score of 0 to 4 had a significantly worse PFS than patients with a score between 5 and 7: 4.0 months (95% CI 3.7-NR) vs. 15 months (95% CI 11.0 – NR),

p=0.003, HR=0.50 (95% CI 0.31-0.81), p=0.005 (Figure 4A). In the case of soluble factors, the prognosis/predictive score separated our population into two groups with different survival: patients with a score of 0 to 3 had a significantly worse PFS compared to patients with a score between 4 and 12: 4.1 months (95% CI 3.5-NR) vs. 17 months (95% CI 3.9 – NR), p=0.005, HR=0.78 (95% CI 0.64-0.95), p=0.012 (Figure 4B). The score integrating both soluble factors and genes that were differentially expressed between baseline and week 13, separated our cohort of cases into two groups with different survival. Patients with a score between 0 and 9 had a significantly worse PFS, compared to patients with a global score of 10 to 19: 4.1 months (95% CI 3.5-NR) vs. 17 months (95% CI 12.0 – NR), p=0.001, HR=0.74 (95% CI 0.60-0.90), p=0.003 (Figure 4C).

The potential predictive value of these molecular scores was further tested using gene and protein expression data obtained from biopsies and peripheral blood samples collected at baseline. A total of 57 patients with paired biopsies and peripheral blood samples were used for this analysis. The gene-based molecular score separated patients into two groups with different PFS: patients with a score of 0 to 3 had a significantly worse PFS, compared to patients with a score between 4 and 7: 2.8 months (95% CI 1.9-6.1) vs. 7.5 months (95% CI 4.4 – 16.0), p<0.001, HR=0.67 (95% CI 0.54-0.84), p<0.001 (Figure 4D). Similarly, soluble factor expression separated our cohort of patients into two groups with different survival: patients with a score of 0 to 6 had a significantly worse PFS compared to patients with a score between 7 and 12: 4.5 months (95% CI 3.3-7.2) vs. 12 months (95% CI 4.0 – NR), p=0.002, HR=0.73 (95% CI 0.62-0.86), p<0.001 (Figure 4E). Finally, the score integrating both soluble factors and genes separated our population into two groups with different survival. Patients with a score between 0 and 12 had a significantly worse PFS, compared to patients with a

global score of 13 to 19: 4.1 months (95% CI 3.3-7.0) vs. 21 months (95% CI 12.0 – NR), p<0.001, HR=0.71 (95% CI 0.62-0.82), p<0.001 (Figure 4F).

Preclinical results

In human tumor-isolated cells and PBMCs from leiomyosarcoma patients, we analyzed the effect of PD-1 inhibitor treatment on the expression of PD-1 and LAG-3 on the cell surface of stimulated $CD4^+$ and $CD8^+$ T cells by flow cytometry, and on the secretion of CXCL10 by the Luminex assay, as a proof of concept to understand whether the changes observed in gene and protein expression levels are due to anti-PD-1 blockage or by the stimulation of the TIME.

In PBMCs, the expression of LAG-3 significantly increased after anti-CD3/CD28 stimulation in $CD8^+$ T cells (0.47 ± 0.38 vs. 35.78 ± 15.24, p=0.001), compared to unstimulated cells (Figure 5A), whereas only a tendency was observed for the surface expression of LAG-3 in $CD4^+$ T cells (0.14 ± 0.07 vs. 11.76 ± 12.14, p=0.065) (Figure 5B). In both $CD8^+$ and $CD4^+$ T cells, the expression of PD-1 at the cell surface significantly increased after stimulation of immune cells (21.9 ± 9.37 vs. 48.32 ± 10.59, p=0.001 and 19.58 ± 2.16 vs. 66.62 ± 15.15, p=0.016, respectively), but this increase was blocked by anti-PD-1 treatment in both $CD8^+$ T cells (48.32 ± 10.59 vs. 13.58 ± 5.50, p=0.004) and $CD4^+$ T cells (66.62 ± 15.15 vs. 29.78 ± 13.74, p=0.004) - Figure 5C and 5D.

In tumor-isolated cells, neither the expression of LAG-3 nor PD-1 changed significantly after anti-CD3/CD28 stimulation (Figure 6A and 6B), although there was a tendency for increased LAG-3 expression in CD8+ T cells (p=0.102) (Figure 6A). The expression of PD-1 was downregulated by treatment with anti-PD-1 antibody in both $CD8^+$ T cells (36.42 ± 21.97 vs.0.48 ± 0.34, p=0.007) (Figure 6C) and $CD4^+$ T cells (31.93 ± 12.07 vs. 0.63 ± 0.63, p=0.001) (Figure 6D).

The expression of CXCL10 was evaluated in PBMCs and tumor-isolated cells. Stimulation of PBMCs with anti-CD3/CD28 increased the release of CXCL10 (19.41 pg/mL ± 13.00 pg/mL vs 577.10 pg/mL ± 210.83 pg/mL, $p<0.001$); however, anti-PD-1 treatment did not alter protein expression levels compared to stimulated PBMCs (Supplementary Figure S5A). In tumor-isolated cells, we did not observe any significant increase in the secretion of CXCL10 after anti-CD3/CD28 stimulation or ICI addition (Supplementary Figure S5B).

DISCUSSION

Our study identified potential molecular mechanisms underlying the response to the combination of ICIs and anti-angiogenic agents in advanced STS, defining a potential prognostic biomarker profile to optimize patient selection for this therapeutic strategy and follow-up. Treatment with anti-angiogenics increased the intratumoral density of $CD8^+$ T cells, along with a dynamic increase in the expression of six genes (*CD86*, *CHI3L1*, *CXCL9*, *CXCL10*, *LAG3*, and *VCAM1*) and the decrease of *NR4A1* expression, and the modulation of 12 soluble factors in peripheral blood. These dynamic changes shed some light on the mechanisms modulated by the combination of anti-angiogenics with PD-1 inhibitors and they can be useful to design novel therapeutic combinations to be tested in future studies in sarcomas. A molecular score, based on the dynamic expression of these seven genes and 12 soluble proteins, significantly separated our study population into two groups with distinct outcomes. To our knowledge, this is the first molecular signature reported for selecting patients with advanced and progressing STS for immunotherapy-based therapy, and it is a potential alternative to the presence of TLS as a predictive biomarker to be tested in future clinical trials with PD-1 inhibitor treatment.

Among the genes that constitute this molecular score, an increase in the expression of *CXCL10* after sunitinib treatment has been previously reported in renal cell carcinoma (RCC).(18) Nonetheless, high expression of this chemokine seems to be associated with worse survival in patients with RCC treated with tyrosine kinase inhibitors (TKIs)(19), suggesting that the survival increase observed in our patients with *CXCL10* augmentation may be due to the combination of sunitinib and ICI anti-PD-1. High expression levels of CXCL10 in the serum significantly correlated with better survival of patients treated with anti-PD-1 antibody for lung carcinoma.(20) Besides, it has also been reported that the axes CXCL9, CXCL10, and CXCL11 (codes ITAC protein)/CXCR3 regulate immune cell migration, differentiation, and activation, leading to intra-tumoral infiltration of $CD8^+$ T cells and tumor suppression.(21-23) Of note, an oncolytic virus linked to CXCL10 has been shown to overcome resistance to anti-PD-1 therapy, inflaming TIME.(24) Thus, it seems reasonable to speculate that in our study, sunitinib increased the expression of CXCL10, attracting $CD8^+$ T cells into the intra-tumoral space, and inflaming the usual 'cold' TIME of sarcomas. Notably, we observed a significant increase in $CD8^+$ T cell density after two cycles of treatment, which validates our initial hypothesis that anti-angiogenic treatment would inflame the sarcoma milieu. More importantly, we found a significant correlation between the dynamic alterations in the density of $CD8^+$ T cells and survival, suggesting that our treatment not only inflamed the tumor microenvironment, but also activated anti-tumor immune response.

However, the increase in the expression levels of CXCL10 may also be due to treatment with a PD-1 inhibitor. Treatment with anti-PD-1 appears to mediate anti-angiogenic effects by increasing the expression levels of CXCL10/11 chemokines and stimulating their binding to the CXCR3 receptor.(20) Nonetheless, in our preclinical experiments,

anti-PD-1 treatment did not induce a significant increase in the expression of CXCL10, suggesting that the increase in the levels of this chemokine may be attributed to the initial induction with the anti-angiogenic agent.

Similar to *CXCL10*, our data showed an increase in the expression of *LAG3* after two cycles of treatment. While there is no direct evidence reported so far on the effect of anti-angiogenic agents or anti-PD-1 on the modulation of the expression levels of LAG-3, it has been described that LAG-3 expression significantly correlated with immune cell infiltration within the tumor(25). This observation suggests that the increase observed in the expression levels of LAG-3 may be a consequence of an increase in the density and activity of $CD8^+$ T cells in the TIME, after anti-angiogenic treatment.

In contrast, the expression of LAG-3 has been associated with worse survival in many tumors(26,27), including sarcomas.(28) In our series, a higher increase in the expression of *LAG3* was associated with better survival, which seems paradoxical, given the immunosuppressive effects of this inhibitory immune checkpoint, but could be explained as a direct consequence of a higher infiltration of activated lymphocytes in the TIME.(29) Moreover, another possible explanation is that LAG-3 plays a role in maintaining immune homeostasis and in preventing excessive inflammation.(30) Higher expression of LAG-3 might indicate a more balanced immune response that effectively controls tumor growth without causing excessive tissue damage. Similar results have been reported in triple-negative breast cancer (TNBC), where high expression of LAG-3 was significantly associated with improved relapse-free survival and overall survival (OS)(31), and in melanoma where high expression of *LAG3* and *LAG3*-hypomethylated tumors showed better OS and improved PFS after ICI treatment, respectively.(32) Noteworthy, in TNBC LAG-3 expression was significantly associated with tumor-infiltrating lymphocytes, supporting the hypothesis that the association between better

PFS and a higher dynamic increase in *LAG3* expression, observed in our data, may be related to the chemotaxis of activated cytotoxic $CD8^+$ T cells into the tumor, which is an accepted prognostic biomarker of better survival(33), rather than to the increase in *LAG3* expression. The increase in the expression levels of *LAG3* might reflect the normal interplay between tumor and immune cells and the subsequent attempt of tumor cells to modulate the immune response in an early stage where a cold tumor turns into an inflamed one.(34)

Likewise, we observed a significant increase in the expression of the activation marker CD86, which underlines the enhanced inflammation within the TIME. Moreover, CD86 is a ligand for another immune checkpoint, CTLA-4.(35) This observation suggests that after inflaming TIME and anti-PD-1 treatment, the expression of this axis is also upregulated and it may also explain the improved outcome observed by the combination of an anti-PD-1 ICI with an anti-CTLA-4 ICI, compared to anti-PD-1 in advanced STS.(5) On the other hand, the VCAM-1 protein mediates the adhesion of lymphocytes, among other immune cells, to the vascular endothelium(36) and it has been shown to benefit immune cell infiltration after anti-angiogenic lenvatinib treatment.(37) Lenvatinib upregulated the expression of VCAM1 early in treatment, which increased the anti-PD-1 therapeutic efficacy, as we observed in our study. Furthermore, it has been reported that the combination treatment of radiotherapy and anti-PD-1 antibodies activates tumor-specific T cells in the TIME, dependent on the upregulation of VCAM-1 protein expression.(38) Regarding *CHI3L1*, it is interesting to observe that in our study higher increased levels of this gene at week 13 were correlated with worse PFS, suggesting that its upregulation could be a mechanism of resistance to treatment. In line with this, it has recently been reported that *CHI3L1* regulates the expression of PD-L1, PD-L2, PD-1, LAG-3, CTLA-4, and TIM3, contributing to an immunosuppressive

microenvironment and tumor progression.(39,40) Therefore, it is plausible that this gene plays an important role in the induction of tumor resistance to immunotherapy-based schemes and its inhibition would increase the efficacy of the treatment. Genome editing or pharmacological studies targeting CHI3L1 should be further developed to test this hypothesis. Finally, *NR4A1* has been shown to promote tumor aggressiveness and maintain immunosuppressive TIME by regulating several mechanisms, including metabolic adaptation.(41) NR4A1 degradation has been shown to promote tumor infiltration of B cells as well as the inhibition of monocytic myeloid-derived suppressor cells, promoting anti-tumor inflammation.(42) Of note, the expression of *NR4A1* decreased significantly after treatment in our study, suggesting that sunitinib treatment may have potentiated ICI activity by suppressing the metabolic pathways regulated by this gene.

Among the several cytokines modulated by treatment, CXCL13 was significantly increased at the beginning of cycle 3, and this increase correlated with better PFS. CXCL13 appears to be particularly relevant in sarcomas because it plays a crucial role in the organization and maintenance of TLS. This protein attracts CXCR5-expressing immune cells, including B cells and $CD4^+$ T cells, to sites where TLSs are formed, contributing to the structural organization of TLS and the generation of an effective antitumor immune response.(43) Besides, the expression of CXCL13 and the presence of TLS have been reported to be both prognostic and predictive biomarkers to improve patient selection for PD-1 inhibitors in STS.(10) In our series, although we observed a significant correlation between the increase in TLS-surrogate chemokine CXCL13 and better PFS, we did not observe a significant correlation between the presence of TLSs and a better outcome. The lack of a significant correlation could be related to the type of material we had available since we only had small biopsies and the likelihood of finding

TLSs in surgical material has been reported to be 6.1 higher than in biopsy.(44) Moreover, it has been reported that TLS is predominantly located at invasive margins, compared to the tumor core.(45) Thus, the fact that we did not control for the areas of biopsy, could have influenced the results obtained. Nonetheless, it is important to mention that our dynamic molecular signature was capable of identifying patients with a higher benefit from immunotherapy-based schemes in a series of cases in which TLSs were unable to predict clinical outcomes. Considering the potential technical limitations mentioned above in detecting TLS, our molecular score signature could be a reliable alternative method to identify patients who could respond to immunomodulation.

Our study has some limitations that are important to be mentioned. First, we used a panel of 2560 genes, which has coverage limitations compared with RNA-Seq. Accordingly, we may have lacked the complete immunomodulatory role of anti-angiogenic and/ or ICI in STS in our study. Additionally, it is important to mention that our second biopsy was performed at week 13, which potentially excluded from the analysis some patients who had already progressed earlier in the study. Thus, our data may not cover the dynamic immune changes observed in patients that quickly progress to anti-angiogenic agents in combination with anti-PD-1 inhibitors. In this sense, it is important to mention that we could not validate our results in an external cohort of cases: to the best of our knowledge, other clinical trials testing anti-PD-1 ICIs in advanced sarcomas did not have scheduled to take two paired biopsies. In the preclinical experiments, we used leiomyosarcoma patient-derived samples, a subtype not included in our clinical trial, which may have introduced some potential bias in our pre-clinical observations, mostly because leiomyosarcoma are typically immune ‘cold’ tumors not responsive to immunomodulation(10), compared to other subtypes very sensitive to ICIs, such as alveolar soft-part sarcoma.(6) Also, we used anti-CD3/CD28 functional

antibodies, which is a direct method to stimulate T-cell activation and propagation(46) and may differ from the effect of anti-angiogenic agents, which act mainly on the TIME, indirectly impacting T-cell responses.(47)

Overall, our results demonstrated the dynamic immunomodulation induced by the combination of an anti-angiogenic agent with a PD-1 inhibitor in STS and described a potential predictive molecular signature for treating patients with anti-PD-1 ICI-based regimens. Future preclinical and clinical studies should focus on the development and testing of therapeutic combinations aiming to increase the expression of CXCL10 an intra-tumoral marker of TME inflamed that could improve the activity of ICIs. In addition, future preclinical studies should address the precise role of anti-angiogenics in the dynamic alterations observed in our study and the specific effects of modulating the expression levels of selected soluble proteins, such as CD30, IL-2R, CCL8, CCL2, CCL22, Eotaxin, and IL-4, on the activity of ICI inhibitors and sarcoma patient outcome, which is not yet fully understood. Furthermore, preclinical studies should also try to understand the increase in the expression of pro-tumoral proteins, such as VEGF-A and IL-8, which may be related to the activation of mechanisms of resistance to TKIs or PD-1 inhibitors. Moreover, the increased expression of LAG-3 after anti-angiogenic and ICI treatment, suggests that clinical trials aiming to inhibit both PD-1 and LAG-3 immune checkpoints, concomitantly or sequentially, are warranted in STS. In line with this, it has already been reported the synergy between anti-PD-1 and anti-LAG-3 ICI and the efficacy of bispecific antibodies targeting LAG-3 and PD-L1 for cancer treatment.(48,49) Additionally, considering the outstanding activity observed between chemotherapy and anti-PD-1 blockage in particular ‘cold’ subtypes of sarcoma, such as leiomyosarcoma(50), it would be of clinical interest to evaluate the potential benefit of adding anti-LAG-3 inhibitors to the combo, at least after anti-PD-1 treatment

completion. Finally, our molecular scores should be further validated in external cohorts and eventually addressed in future clinical trials testing immunotherapy combos as a tool for prognostication and predicting patient outcomes. Owing to the non-invasive nature of liquid biopsy, the soluble protein-based signature identified in our study deserves prioritization for future validations.

Acknowledgments: The authors would like to thank Patricio Ledesma for Data Management. The authors would like to thank the Sarcoma Foundation of America, Asociación Iker, and Spanish Group for Research on Sarcomas (GEIS) for supporting this study. David S. Moura was the recipient of a Sara Borrell postdoctoral fellowship funded by the National Institute of Health Carlos III (ISCIII) (CD20/00155). The authors also thank the SELNET Project. SELNET received funding from the European Union's Horizon 2020 Research and Innovation Program under grant agreement Nº. 825806. The authors would like to thank Charles University, project GA UK No. 94323, and the Ministry of Health, Czech Republic, project AZV NU23J-08-00031, for supporting the study. The authors would like to thank BMS and Pfizer for allowing execution of the IMMUNOSARC trial. The authors would like to thank the huge effort

from the patients, who accepted the collection of mandatory biopsies and peripheral blood samples.

REFERENCES

1. Tang F, Tie Y, Wei Y-Q, Tu C-Q, Wei X-W. Targeted and immuno-based therapies in sarcoma: mechanisms and advances in clinical trials. *Biochimica et Biophysica Acta (BBA) - Reviews on Cancer* 2021;**1876**(2):188606 doi https://doi.org/10.1016/j.bbcan.2021.188606.
2. Martín-Broto J, Moura DS, Van Tine BA. Facts and Hopes in Immunotherapy of Soft-Tissue Sarcomas. *Clin Cancer Res* 2020;**26**(22):5801-8 doi 10.1158/1078-0432.Ccr-19-3335.
3. Martin-Broto J, Hindi N, Grignani G, Martinez-Trufero J, Redondo A, Valverde C, *et al.* Nivolumab and sunitinib combination in advanced soft tissue sarcomas: a multicenter, single-arm, phase Ib/II trial. *Journal for ImmunoTherapy of Cancer* 2020;**8**(2):e001561 doi 10.1136/jitc-2020-001561.
4. Wilky BA, Trucco MM, Subhawong TK, Florou V, Park W, Kwon D, *et al.* Axitinib plus pembrolizumab in patients with advanced sarcomas including alveolar soft-part sarcoma: a single-centre, single-arm, phase 2 trial. *The Lancet Oncology* 2019;**20**(6):837-48 doi 10.1016/s1470-2045(19)30153-6.
5. D'Angelo SP, Mahoney MR, Van Tine BA, Atkins J, Milhem MM, Jahagirdar BN, *et al.* Nivolumab with or without ipilimumab treatment for metastatic sarcoma (Alliance A091401): two open-label, non-comparative, randomised,

phase 2 trials. *Lancet Oncol* 2018;**19**(3):416-26 doi 10.1016/s1470-2045(18)30006-8.
6. Hindi N, Razak A, Rosenbaum E, Jonczak E, Hamacher R, Rutkowski P, *et al.* Efficacy of immune checkpoint inhibitors in alveolar soft-part sarcoma: results from a retrospective worldwide registry. *ESMO Open* 2023;**8**(6):102045 doi 10.1016/j.esmoop.2023.102045.
7. Motz GT, Coukos G. The parallel lives of angiogenesis and immunosuppression: cancer and other tales. *Nat Rev Immunol* 2011;**11**(10):702-11 doi 10.1038/nri3064.
8. Freeman MR, Schneck FX, Gagnon ML, Corless C, Soker S, Niknejad K, *et al.* Peripheral blood T lymphocytes and lymphocytes infiltrating human cancers express vascular endothelial growth factor: a potential role for T cells in angiogenesis. *Cancer Res* 1995;**55**(18):4140-5.
9. Huang MT, Dai YS, Chou YB, Juan YH, Wang CC, Chiang BL. Regulatory T cells negatively regulate neovasculature of airway remodeling via DLL4-Notch signaling. *J Immunol* 2009;**183**(7):4745-54 doi 10.4049/jimmunol.0804371.
10. Petitprez F, de Reyniès A, Keung EZ, Chen TW-W, Sun C-M, Calderaro J, *et al.* B cells are associated with survival and immunotherapy response in sarcoma. *Nature* 2020;**577**(7791):556-60 doi 10.1038/s41586-019-1906-8.
11. Martin-Broto J, Stacchiotti S, Lopez-Pousa A, Redondo A, Bernabeu D, de Alava E, *et al.* Pazopanib for treatment of advanced malignant and dedifferentiated solitary fibrous tumour: a multicentre, single-arm, phase 2 trial. *Lancet Oncol* 2019;**20**(1):134-44 doi 10.1016/s1470-2045(18)30676-4.
12. Melero I, Villalba-Esparza M, Recalde-Zamacona B, Jiménez-Sánchez D, Teijeira Á, Argueta A, *et al.* Neutrophil Extracellular Traps, Local IL-8 Expression, and Cytotoxic T-Lymphocyte Response in the Lungs of Patients With Fatal COVID-19. *Chest* 2022;**162**(5):1006-16 doi 10.1016/j.chest.2022.06.007.
13. de Andrea CE, Ochoa MC, Villalba-Esparza M, Teijeira Á, Schalper KA, Abengozar-Muela M, *et al.* Heterogenous presence of neutrophil extracellular traps in human solid tumours is partially dependent on IL-8. *J Pathol* 2021;**255**(2):190-201 doi 10.1002/path.5753.
14. Martinez-Valbuena I, Valenti-Azcarate R, Amat-Villegas I, Riverol M, Marcilla I, de Andrea CE, *et al.* Amylin as a potential link between type 2 diabetes and alzheimer disease. *Ann Neurol* 2019;**86**(4):539-51 doi 10.1002/ana.25570.
15. Abengozar-Muela M, Esparza MV, Garcia-Ros D, Vásquez CE, Echeveste JI, Idoate MA, *et al.* Diverse immune environments in human lung tuberculosis granulomas assessed by quantitative multiplexed immunofluorescence. *Mod Pathol* 2020;**33**(12):2507-19 doi 10.1038/s41379-020-0600-6.
16. Newman AM, Steen CB, Liu CL, Gentles AJ, Chaudhuri AA, Scherer F, *et al.* Determining cell type abundance and expression from bulk tissues with digital cytometry. *Nature Biotechnology* 2019;**37**(7):773-82 doi 10.1038/s41587-019-0114-2.
17. Newman AM, Liu CL, Green MR, Gentles AJ, Feng W, Xu Y, *et al.* Robust enumeration of cell subsets from tissue expression profiles. *Nature Methods* 2015;**12**(5):453-7 doi 10.1038/nmeth.3337.
18. Xu W, Puligandla M, Manola J, Bullock AJ, Tamasauskas D, McDermott DF, *et al.* Angiogenic Factor and Cytokine Analysis among Patients Treated with Adjuvant VEGFR TKIs in Resected Renal Cell Carcinoma. *Clin Cancer Res* 2019;**25**(20):6098-106 doi 10.1158/1078-0432.Ccr-19-0818.

19. Esteban E, Exposito F, Crespo G, Lambea J, Pinto A, Puente J, *et al.* Circulating Levels of the Interferon-γ-Regulated Chemokines CXCL10/CXCL11, IL-6 and HGF Predict Outcome in Metastatic Renal Cell Carcinoma Patients Treated with Antiangiogenic Therapy. *Cancers (Basel)* 2021;**13**(11) doi 10.3390/cancers13112849.
20. Mitsuhashi A, Kondoh K, Horikawa K, Koyama K, Nguyen NT, Afroj T, *et al.* Programmed death (PD)-1/PD-ligand 1 blockade mediates antiangiogenic effects by tumor-derived CXCL10/11 as a potential predictive biomarker. *Cancer Sci* 2021;**112**(12):4853-66 doi 10.1111/cas.15161.
21. Yan W, Qiu L, Yang M, Xu A, Ma M, Yuan Q, *et al.* CXCL10 mediates CD8+ T cells to facilitate vessel normalization and improve the efficacy of cetuximab combined with PD-1 checkpoint inhibitors in colorectal cancer. *Cancer Letters* 2023;**567**:216263 doi https://doi.org/10.1016/j.canlet.2023.216263.
22. Reschke R, Yu J, Flood BA, Higgs EF, Hatogai K, Gajewski TF. Immune cell and tumor cell-derived CXCL10 is indicative of immunotherapy response in metastatic melanoma. *Journal for ImmunoTherapy of Cancer* 2021;**9**(9):e003521 doi 10.1136/jitc-2021-003521.
23. House IG, Savas P, Lai J, Chen AXY, Oliver AJ, Teo ZL, *et al.* Macrophage-Derived CXCL9 and CXCL10 Are Required for Antitumor Immune Responses Following Immune Checkpoint Blockade. *Clinical Cancer Research* 2020;**26**(2):487-504 doi 10.1158/1078-0432.Ccr-19-1868.
24. Li X, Lu M, Yuan M, Ye J, Zhang W, Xu L, *et al.* CXCL10-armed oncolytic adenovirus promotes tumor-infiltrating T-cell chemotaxis to enhance anti-PD-1 therapy. *Oncoimmunology* 2022;**11**(1):2118210 doi 10.1080/2162402x.2022.2118210.
25. Klümper N, Ralser DJ, Bawden EG, Landsberg J, Zarbl R, Kristiansen G, *et al.* LAG3 (LAG-3, CD223) DNA methylation correlates with LAG3 expression by tumor and immune cells, immune cell infiltration, and overall survival in clear cell renal cell carcinoma. *J Immunother Cancer* 2020;**8**(1) doi 10.1136/jitc-2020-000552.
26. Takamatsu K, Tanaka N, Hakozaki K, Takahashi R, Teranishi Y, Murakami T, *et al.* Profiling the inhibitory receptors LAG-3, TIM-3, and TIGIT in renal cell carcinoma reveals malignancy. *Nature Communications* 2021;**12**(1):5547 doi 10.1038/s41467-021-25865-0.
27. Hasanov E, Peterson CB, Matin SF, Wood CG, Sircar K, Tannir NM, *et al.* Hypoxia signaling and immune infiltration in a presurgical trial of sunitinib in patients with clear cell renal cell carcinoma (RCC). *Journal of Clinical Oncology* 2019;**37**(15_suppl):e16115-e doi 10.1200/JCO.2019.37.15_suppl.e16115.
28. Li R, Qiu J, Zhang Z, Qu C, Tang Z, Yu W, *et al.* Prognostic significance of Lymphocyte-activation gene 3 (LAG3) in patients with solid tumors: a systematic review, meta-analysis and pan-cancer analysis. *Cancer Cell International* 2023;**23**(1):306 doi 10.1186/s12935-023-03157-5.
29. Grosso JF, Kelleher CC, Harris TJ, Maris CH, Hipkiss EL, De Marzo A, *et al.* LAG-3 regulates CD8+ T cell accumulation and effector function in murine self- and tumor-tolerance systems. *J Clin Invest* 2007;**117**(11):3383-92 doi 10.1172/jci31184.
30. Zhao H, Wu L, Yan G, Chen Y, Zhou M, Wu Y, *et al.* Inflammation and tumor progression: signaling pathways and targeted intervention. *Signal Transduction and Targeted Therapy* 2021;**6**(1):263 doi 10.1038/s41392-021-00658-5.

31. Stovgaard ES, Kümler I, List-Jensen K, Roslind A, Christensen IJ, Høgdall E, *et al.* Prognostic and Clinicopathologic Associations of LAG-3 Expression in Triple-negative Breast Cancer. *Appl Immunohistochem Mol Morphol* 2022;**30**(1):62-71 doi 10.1097/pai.0000000000000954.
32. Fröhlich A, Sirokay J, Fietz S, Vogt TJ, Dietrich J, Zarbl R, *et al.* Molecular, clinicopathological, and immune correlates of LAG3 promoter DNA methylation in melanoma. *eBioMedicine* 2020;**59**:102962 doi https://doi.org/10.1016/j.ebiom.2020.102962.
33. Fumet JD, Richard C, Ledys F, Klopfenstein Q, Joubert P, Routy B, *et al.* Prognostic and predictive role of CD8 and PD-L1 determination in lung tumor tissue of patients under anti-PD-1 therapy. *Br J Cancer* 2018;**119**(8):950-60 doi 10.1038/s41416-018-0220-9.
34. Burugu S, Gao D, Leung S, Chia SK, Nielsen TO. LAG-3+ tumor infiltrating lymphocytes in breast cancer: clinical correlates and association with PD-1/PD-L1+ tumors. *Ann Oncol* 2017;**28**(12):2977-84 doi 10.1093/annonc/mdx557.
35. Vandenborre K, Van Gool SW, Kasran A, Ceuppens JL, Boogaerts MA, Vandenberghe P. Interaction of CTLA-4 (CD152) with CD80 or CD86 inhibits human T-cell activation. *Immunology* 1999;**98**(3):413-21 doi 10.1046/j.1365-2567.1999.00888.x.
36. Deem TL, Cook-Mills JM. Vascular cell adhesion molecule 1 (VCAM-1) activation of endothelial cell matrix metalloproteinases: role of reactive oxygen species. *Blood* 2004;**104**(8):2385-93 doi 10.1182/blood-2004-02-0665.
37. Yang J, Guo Z, Song M, Pan Q, Zhao J, Huang Y, *et al.* Lenvatinib improves anti-PD-1 therapeutic efficacy by promoting vascular normalization via the NRP-1-PDGFRβ complex in hepatocellular carcinoma. *Frontiers in Immunology* 2023;**14** doi 10.3389/fimmu.2023.1212577.
38. Kim S, Sanders PD, Weihe E, Purcell T, Kato S, Patel S, *et al.* Analysis of Immune Correlates Using Anti-PD-1 Checkpoint Blockade Immunotherapy Combined With Stereotactic Body Radiation Therapy. *International Journal of Radiation Oncology, Biology, Physics* 2017;**99**(2):E602-E3 doi 10.1016/j.ijrobp.2017.06.2051.
39. Ma B, Akosman B, Kamle S, Lee CM, He CH, Koo JS, *et al.* CHI3L1 regulates PD-L1 and anti-CHI3L1-PD-1 antibody elicits synergistic antitumor responses. *J Clin Invest* 2021;**131**(21) doi 10.1172/jci137750.
40. Ma B, Kamle S, Akosman B, Khan H, Lee C-M, Lee CG, *et al.* CHI3L1 enhances melanoma lung metastasis via regulation of T cell co-stimulators and CTLA-4/B7 axis. *Frontiers in Immunology* 2022;**13** doi 10.3389/fimmu.2022.1056397.
41. Deng S, Chen B, Huo J, Liu X. Therapeutic potential of NR4A1 in cancer: Focus on metabolism. *Front Oncol* 2022;**12**:972984 doi 10.3389/fonc.2022.972984.
42. Wang L, Xiao Y, Luo Y, Master RP, Mo J, Kim MC, *et al.* PROTAC-mediated NR4A1 degradation as a novel strategy for cancer immunotherapy. *J Exp Med* 2024;**221**(3) doi 10.1084/jem.20231519.
43. Ukita M, Hamanishi J, Yoshitomi H, Yamanoi K, Takamatsu S, Ueda A, *et al.* CXCL13-producing CD4+ T cells accumulate in the early phase of tertiary lymphoid structures in ovarian cancer. *JCI Insight* 2022;**7**(12) doi 10.1172/jci.insight.157215.
44. Vanhersecke L, Bougouin A, Crombé A, Brunet M, Sofeu C, Parrens M, *et al.* Standardized Pathology Screening of Mature Tertiary Lymphoid Structures in

Cancers. *Laboratory Investigation* 2023;**103**(5):100063 doi https://doi.org/10.1016/j.labinv.2023.100063.
45. Kasikova L, Rakova J, Hensler M, Lanickova T, Tomankova J, Pasulka J, *et al.* Tertiary lymphoid structures and B cells determine clinically relevant T cell phenotypes in ovarian cancer. *Nature Communications* 2024;**15**(1):2528 doi 10.1038/s41467-024-46873-w.
46. Borcinova M, Bartolini R, Foley LK, Novak V, Taborska P, Stakheev D, *et al.* Distinct leukocyte populations and cytokine secretion profiles define tumoral and peritumoral areas in renal cell carcinoma. *Translational Oncology* 2024;**42**:101891 doi https://doi.org/10.1016/j.tranon.2024.101891.
47. Kashyap AS, Schmittnaegel M, Rigamonti N, Pais-Ferreira D, Mueller P, Buchi M, *et al.* Optimized antiangiogenic reprogramming of the tumor microenvironment potentiates CD40 immunotherapy. *Proceedings of the National Academy of Sciences* 2020;**117**(1):541-51 doi doi:10.1073/pnas.1902145116.
48. Woo SR, Turnis ME, Goldberg MV, Bankoti J, Selby M, Nirschl CJ, *et al.* Immune inhibitory molecules LAG-3 and PD-1 synergistically regulate T-cell function to promote tumoral immune escape. *Cancer Res* 2012;**72**(4):917-27 doi 10.1158/0008-5472.Can-11-1620.
49. Kraman M, Faroudi M, Allen NL, Kmiecik K, Gliddon D, Seal C, *et al.* FS118, a Bispecific Antibody Targeting LAG-3 and PD-L1, Enhances T-Cell Activation Resulting in Potent Antitumor Activity. *Clin Cancer Res* 2020;**26**(13):3333-44 doi 10.1158/1078-0432.Ccr-19-3548.
50. Broto JM, Beveridge RD, Moura D, Ramos R, Martinez-Trufero J, Carrasco-Garcia I, *et al.* ImmunoSarc2: A Spanish Sarcoma Group (GEIS) phase Ib trial of doxorubicin and dacarbazine plus nivolumab in first line treatment of advanced leiomyosarcoma. *Journal of Clinical Oncology* 2023;**41**(16_suppl):11502- doi 10.1200/JCO.2023.41.16_suppl.11502.

FIGURE LEGENDS

Figure 1. Immune cell densities at baseline and week 13: A) CD3, B) CD8, C) CD4, D) CD20, E) CD66b, F) CD68 and G) CD138.

Figure 2. Dynamic modulation of the abundance of $CD8^+$ cells determined by CIBERSORTx. Density levels between baseline and week 13 of B cells (A) and prognostic value of the dynamic modulation of B cells abundance (B). Density levels between baseline and week 13 of $CD4^+$ T cells (C) and prognostic value of the dynamic modulation of $CD4^+$ T cells abundance (D). Density levels between baseline and week

13 of $CD8^+$ T cells (E) and prognostic value of the dynamic modulation of $CD8^+$ T cells abundance (F). Density levels between baseline and week 13 of monocytes (G) and prognostic value of the dynamic modulation of monocyte abundance (H). PFS cut-off was defined as 5.6 months and calculated by MAXSTAT. Significance was defined as $p<0.05$ and calculated by Wilcoxon paired test.

Figure 3. Correlation between progression-free survival (PFS) and the dynamic alteration in the expression of soluble proteins in plasma samples. Samples were collected at baseline and week 13 (Cycle 3, day 1). PFS cut-off was defined as 7.2 months and calculated by MAXSTAT. Significance was defined as $p<0.05$ and calculated by Wilcoxon paired test. Concentration is represented as log2 (pg/mL). CXCL123: BLC; CXCL11: I-TAC; CXCL10: IP-10; CCL2: MCP-1; CCL8: MCP-2; and CCL22: MDC.

Figure 4. Progression-free survival according to the dynamic molecular scores. A) gene-based score; B) soluble proteins-based score; C) score integrating both the 7 genes and the 12 soluble proteins that showed significantly different expression levels between baseline and week 13; D) gene-based score applied to transcriptomic data determined in baseline biopsies; E) soluble protein-based score applied to Luminex results determined in plasma samples collected at baseline and F) integrative molecular score (7 genes and 12 proteins) applied to baseline gene and protein expression data. Samples were collected at baseline and week 13 (Cycle 3, day 1). MAXSTAR tool was used to calculate optimal cut-offs.

Figure 5. Effect of T-cell stimulation and anti-PD-1 treatment on the expression of LAG-3 and PD-1 in $CD4^+$ and $CD8^+$ T cells from peripheral blood. Flow cytometry analysis of the expression of A) LAG-3 in $CD8^+$ T cells; B) LAG-3 in $CD4^+$ T cells; C)

PD-1 in $CD8^+$ T cells and D) PD-1 in $CD4^+$ T cells. Significance was defined as $p<0.05$ (Students t-test).

Figure 6. Effect of T-cell stimulation and anti-PD-1 treatment in the expression of LAG-3 and PD-1 in intra-tumoral $CD4^+$ and $CD8^+$ T cells. Flow cytometry analysis of the expression of A) LAG-3 in $CD8^+$ T cells; B) LAG-3 in $CD4^+$ T cells; C) PD-1 in $CD8^+$ T cells and D) PD-1 in $CD4^+$ T cells. Significance was defined as $p<0.05$ (Students t-test).

Figure 1

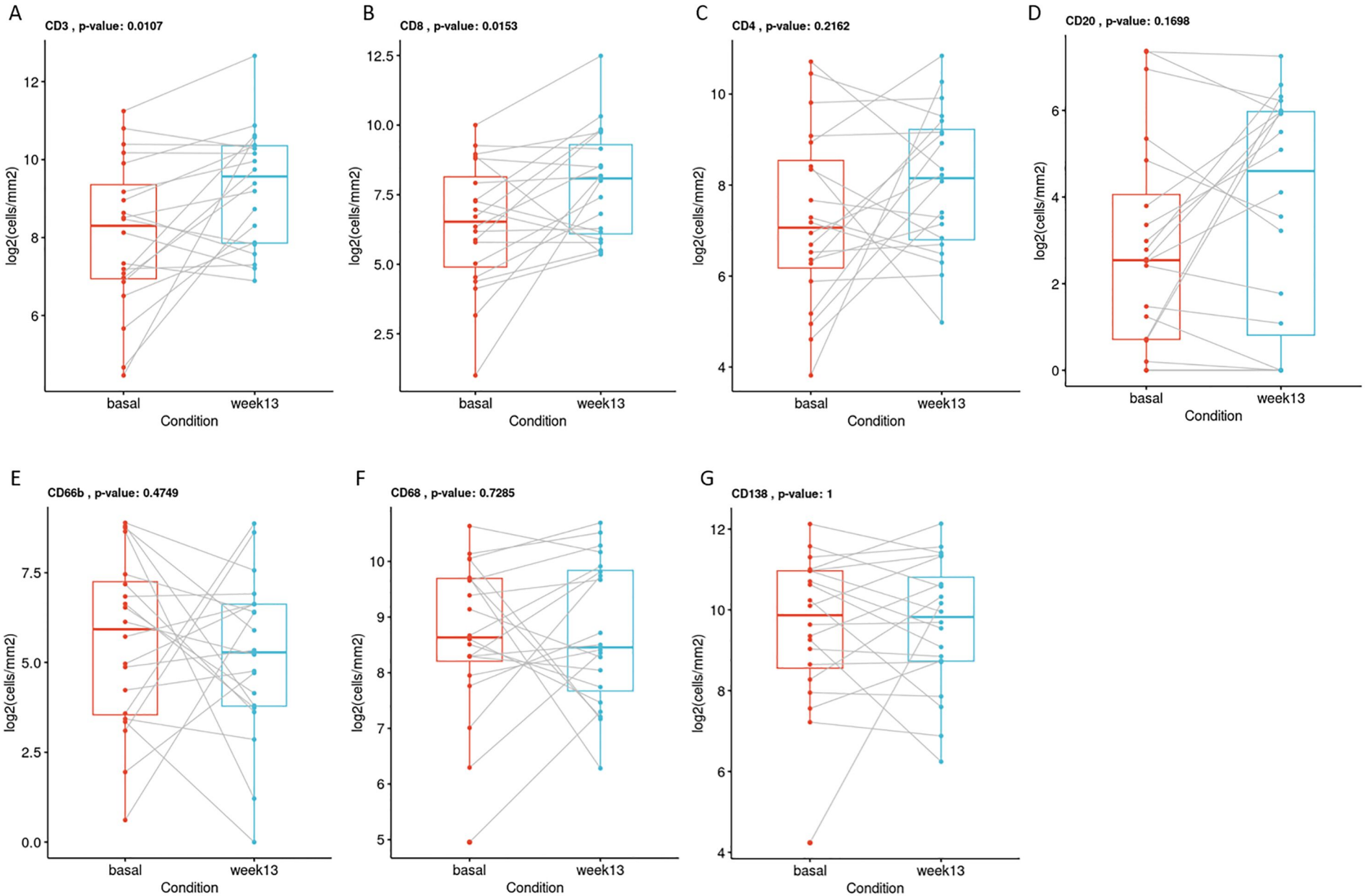

Figure 2

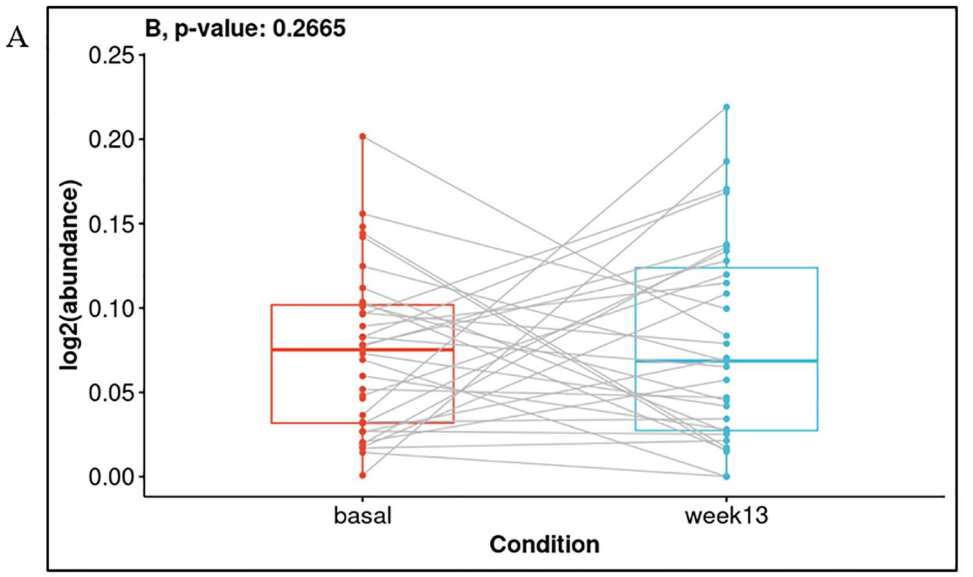

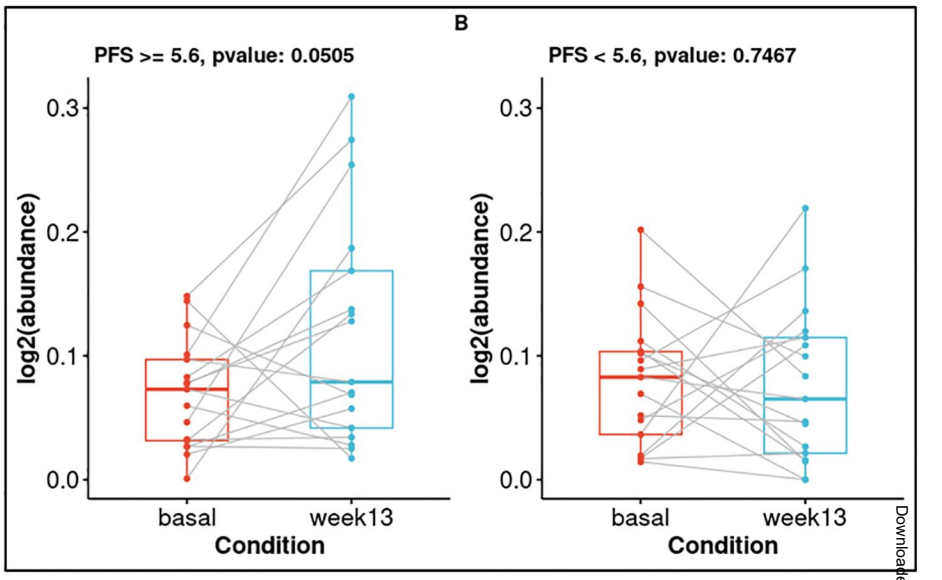

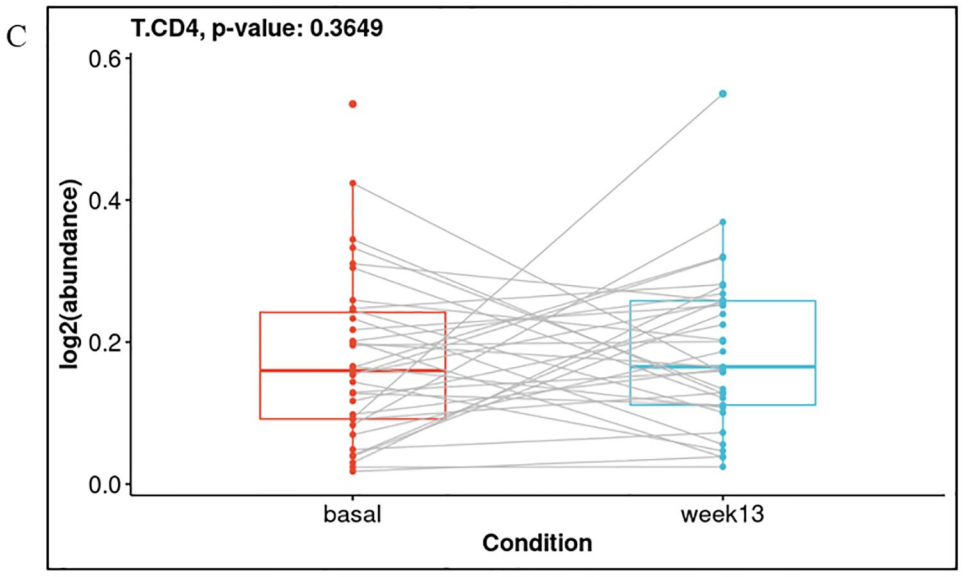

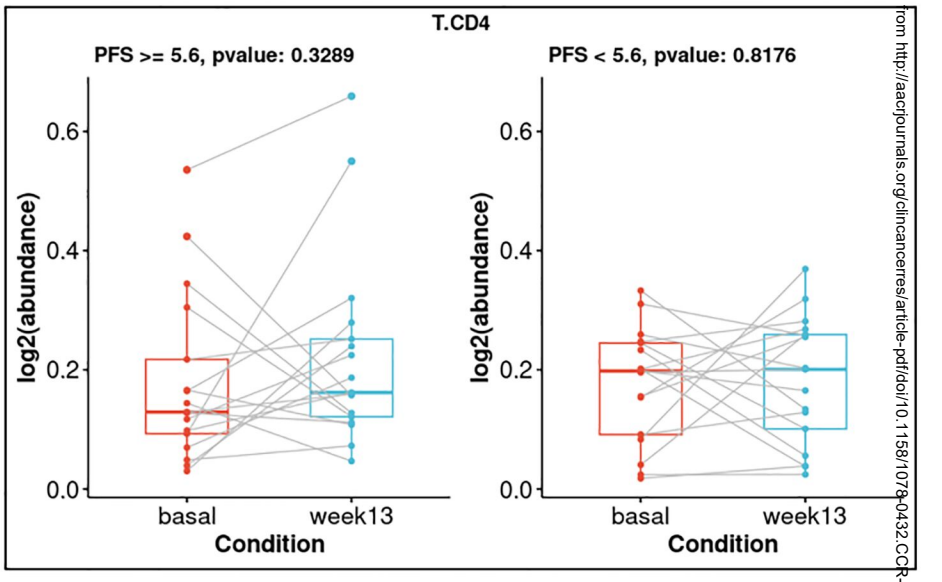

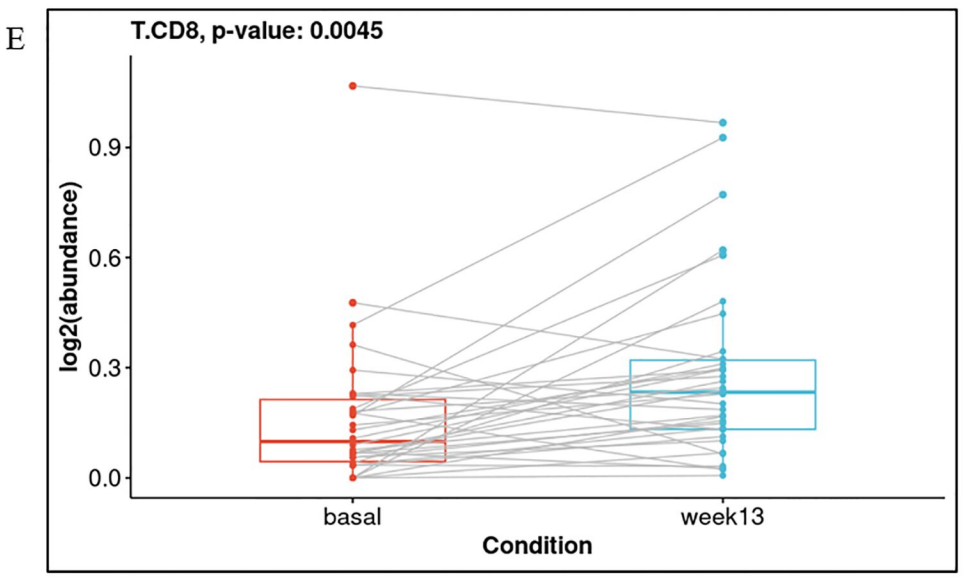

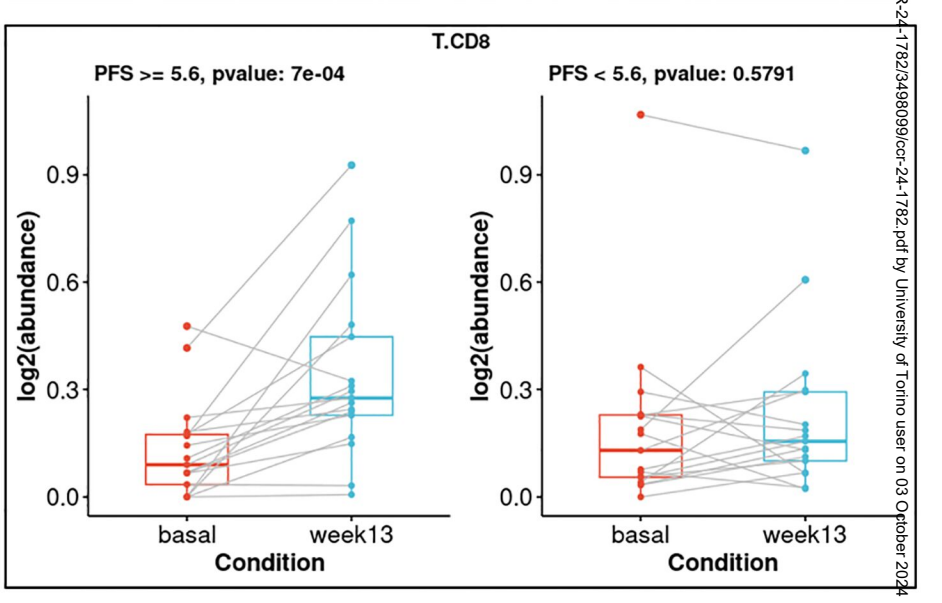

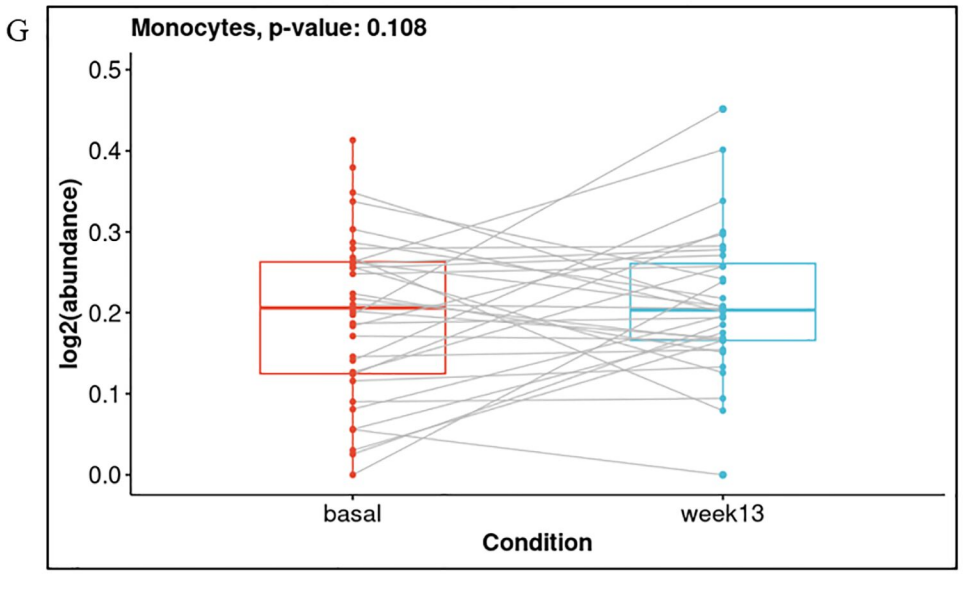

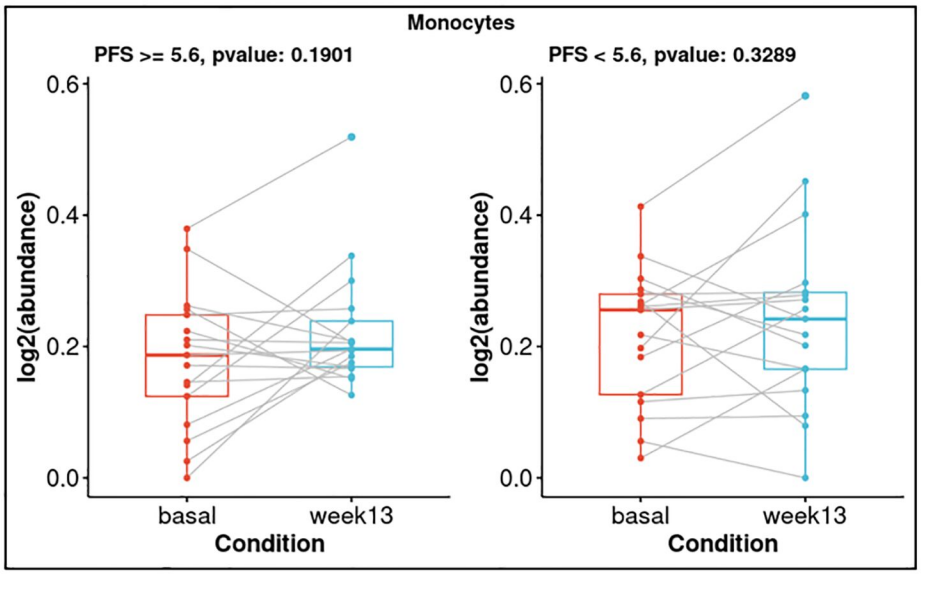

Figure 3

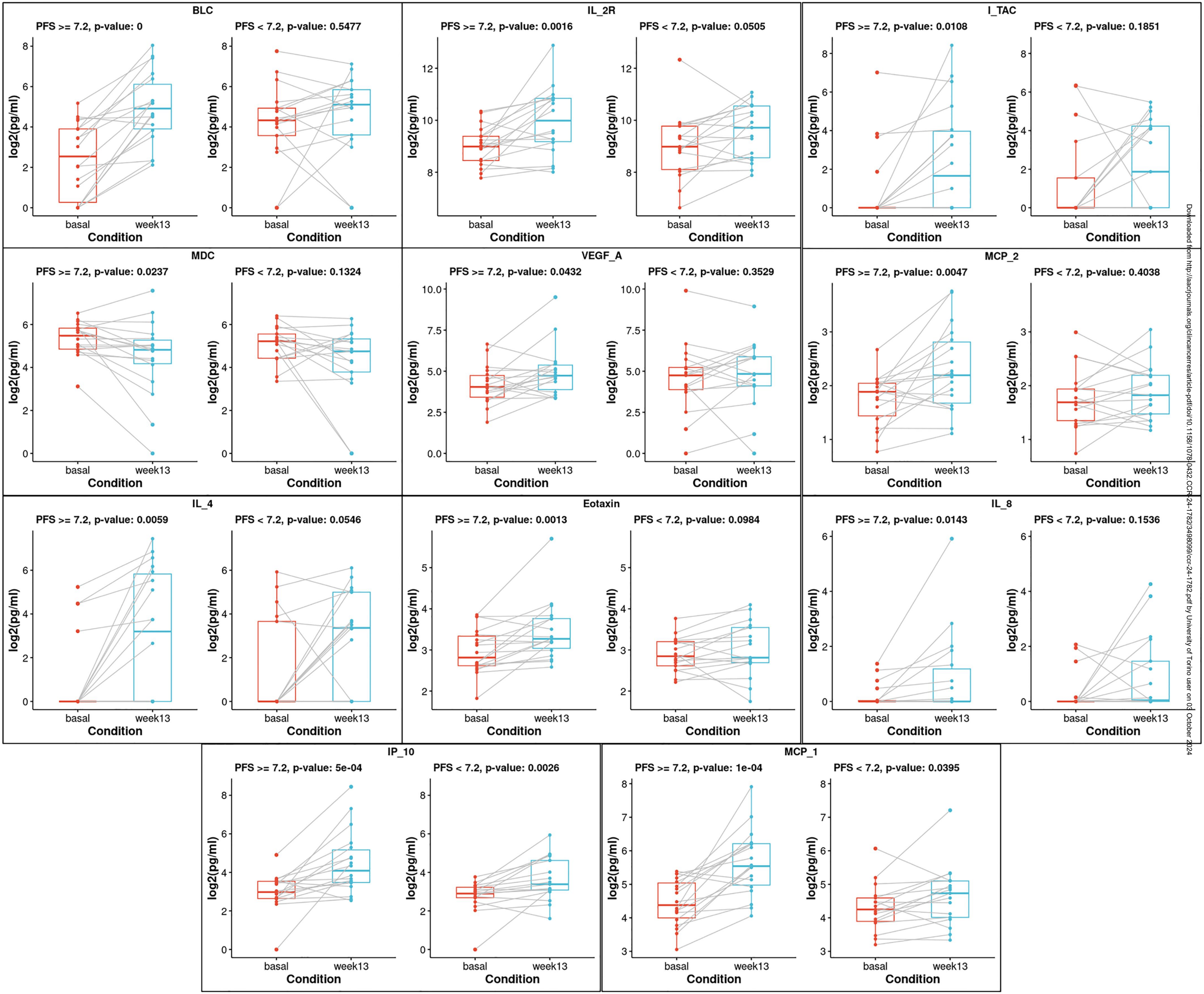

Figure 4

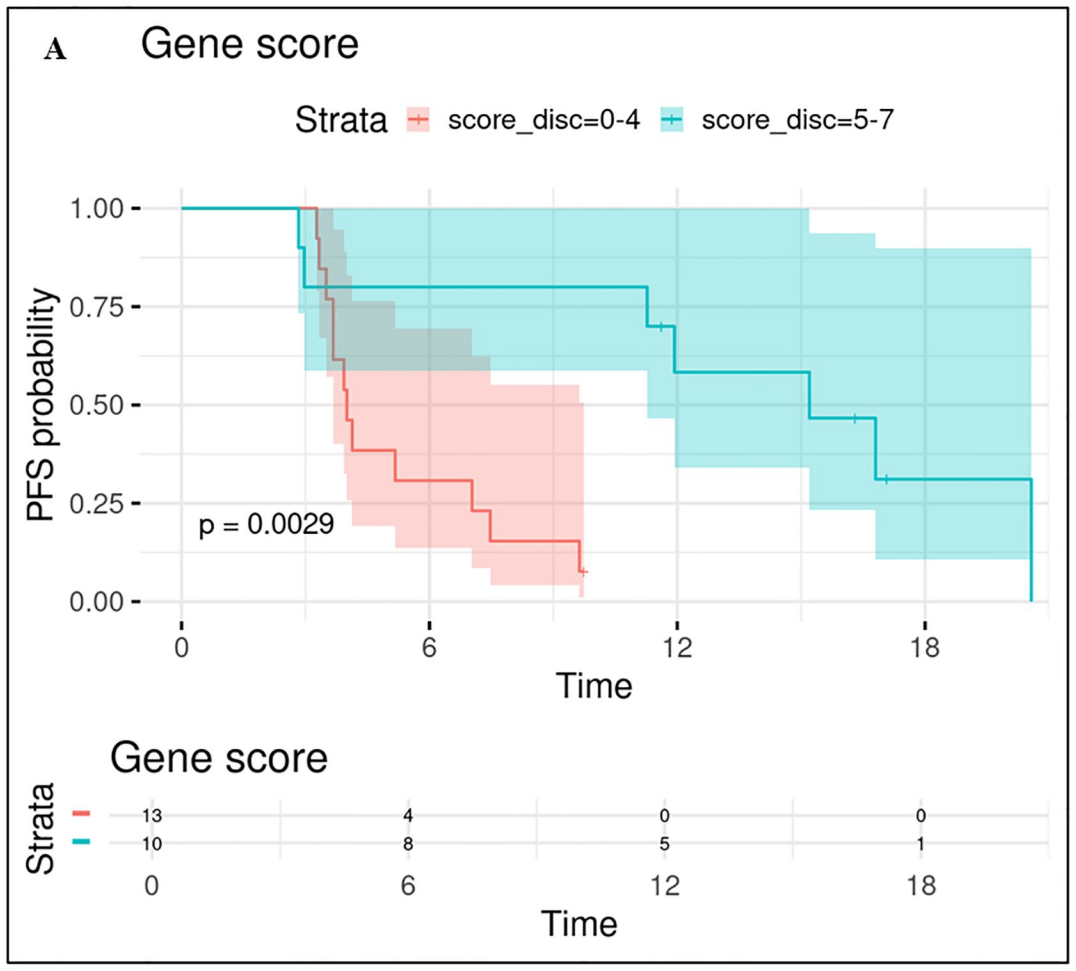

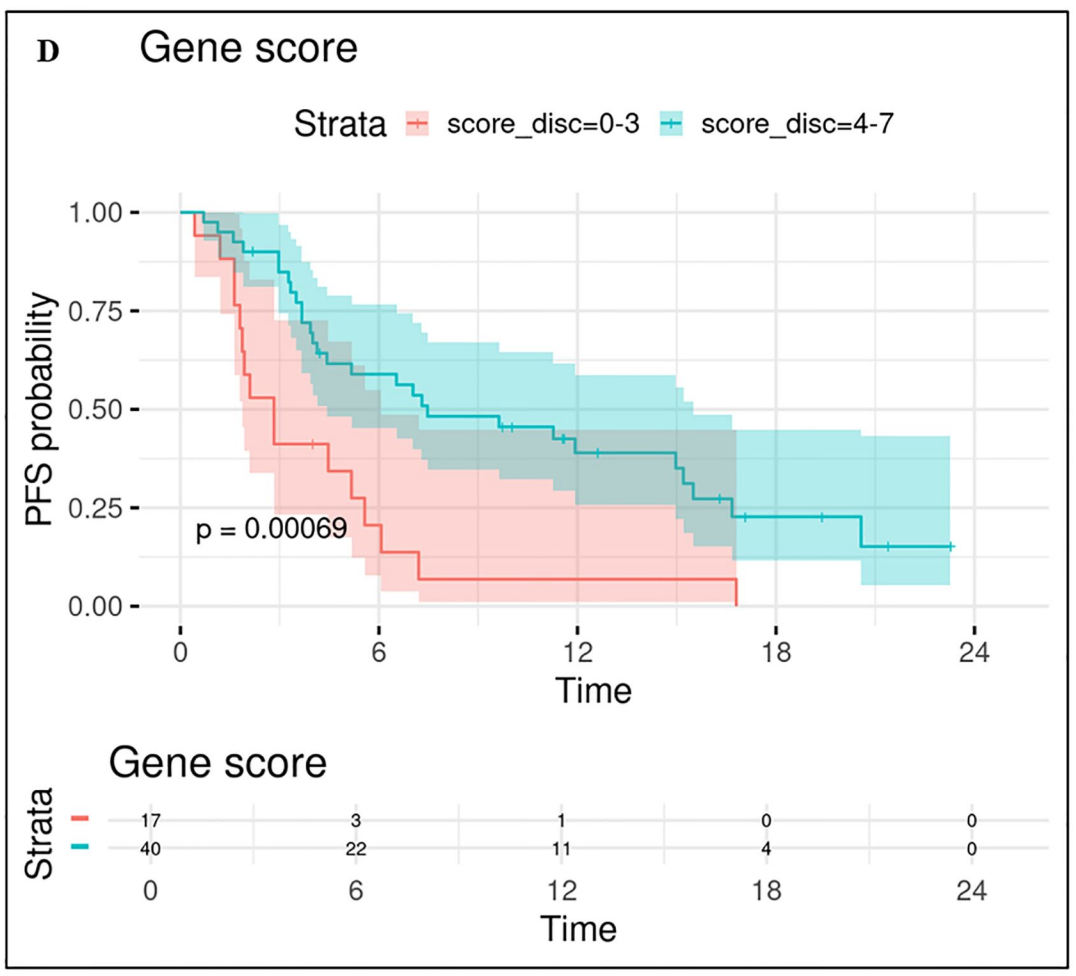

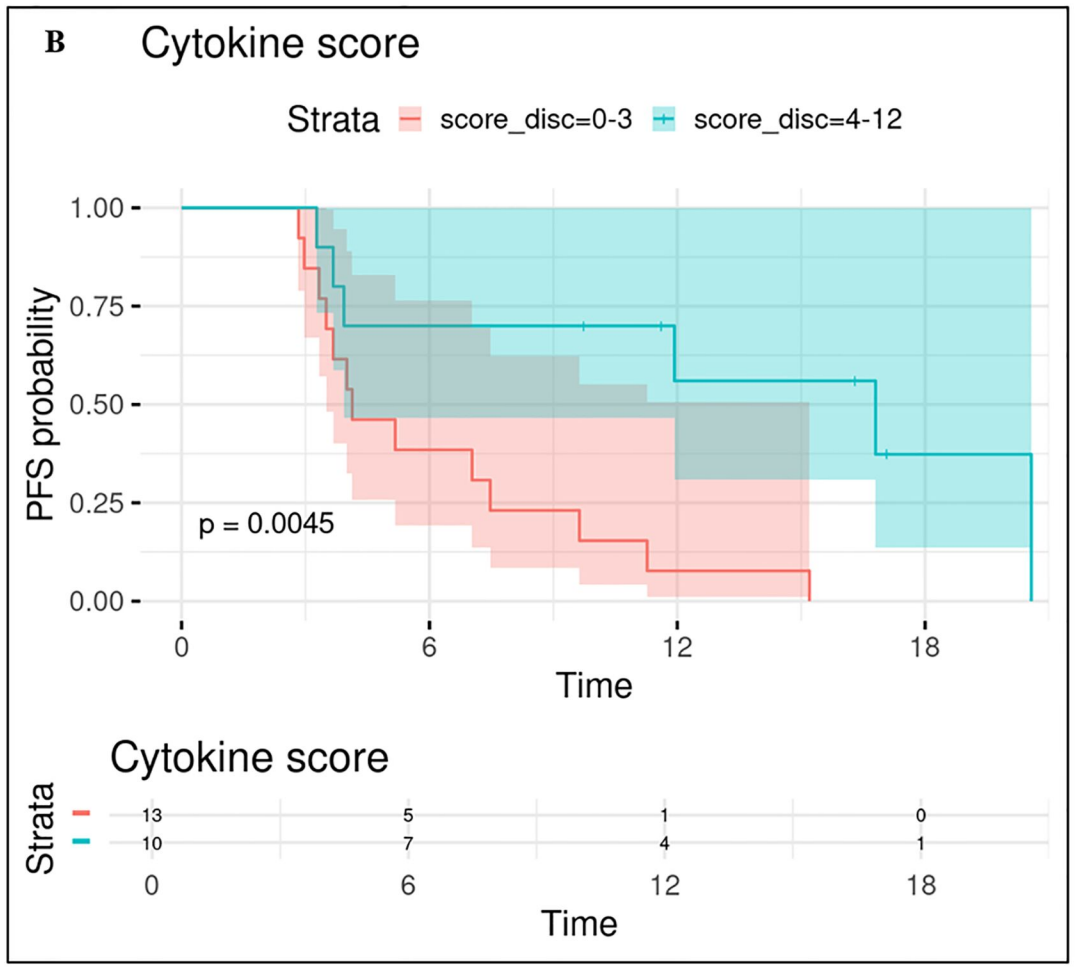

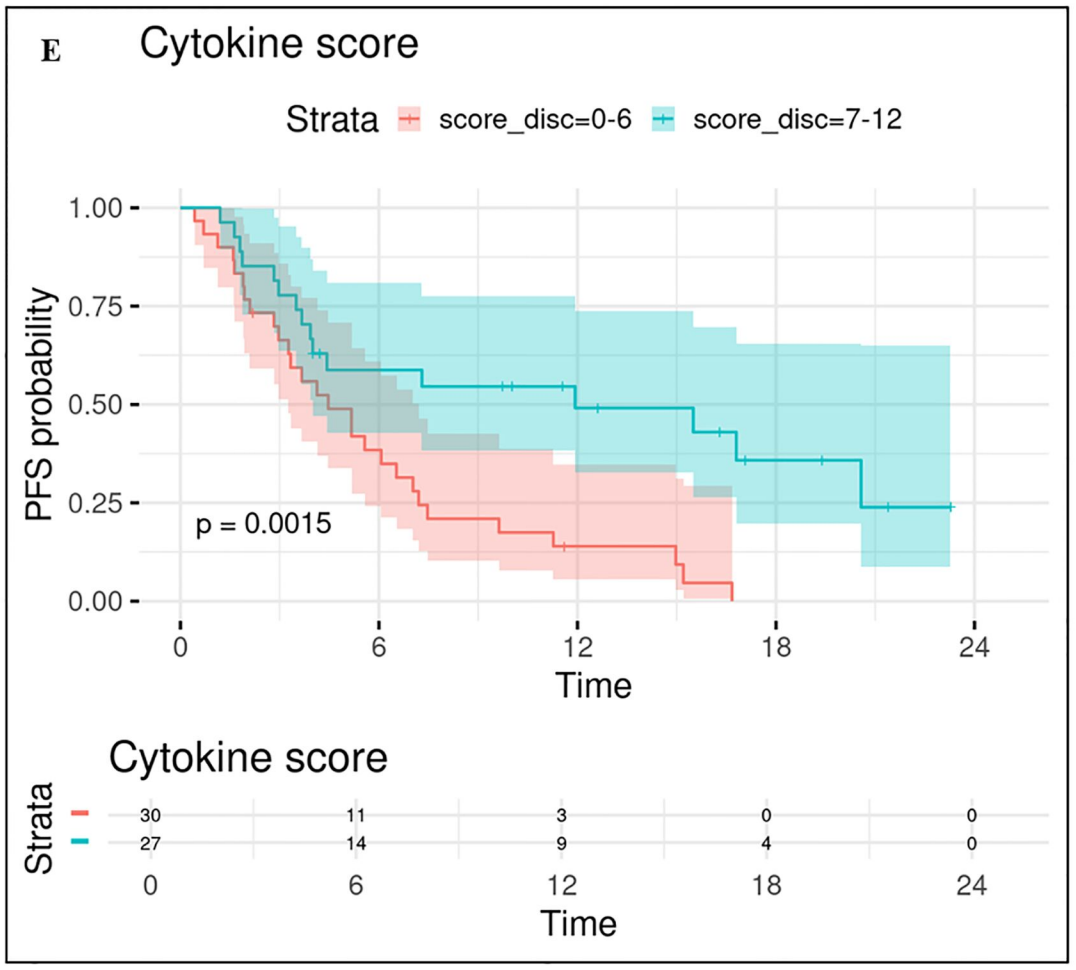

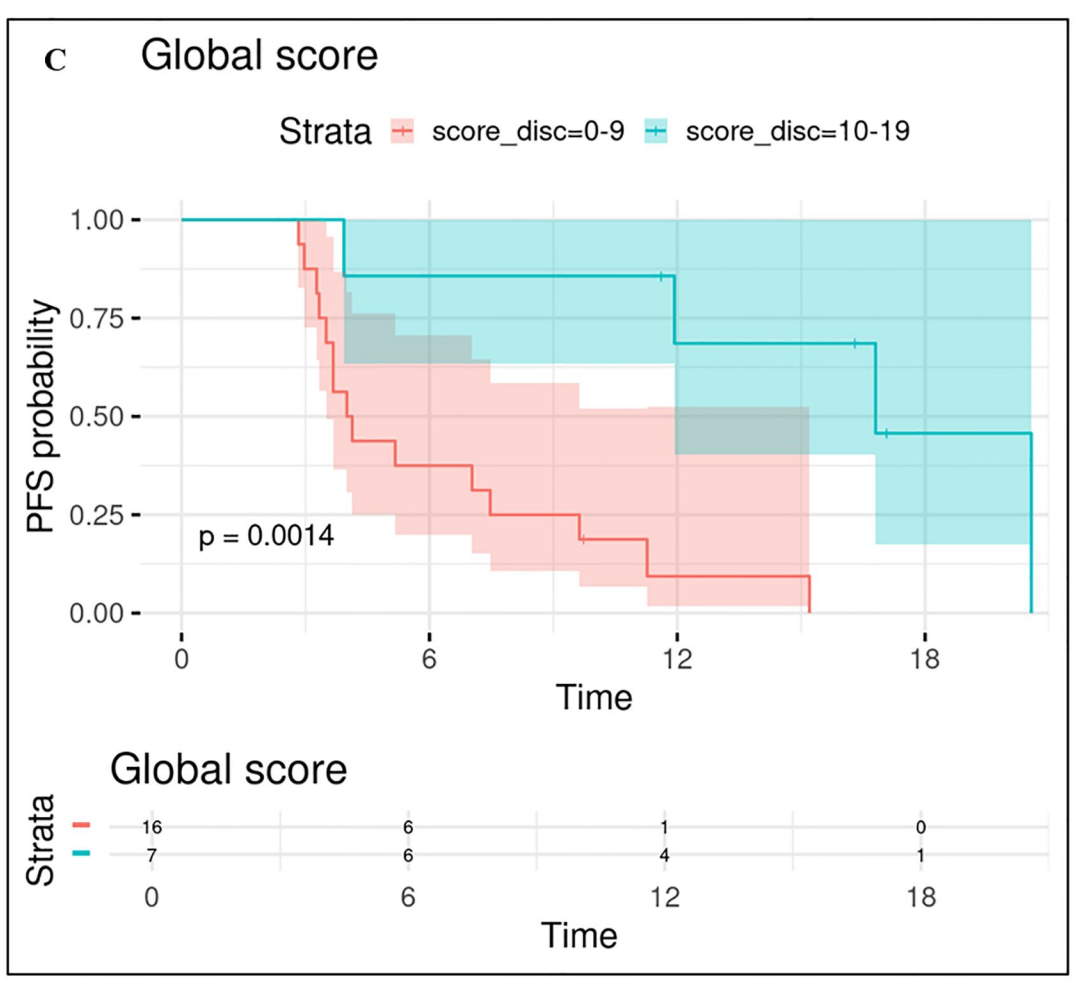

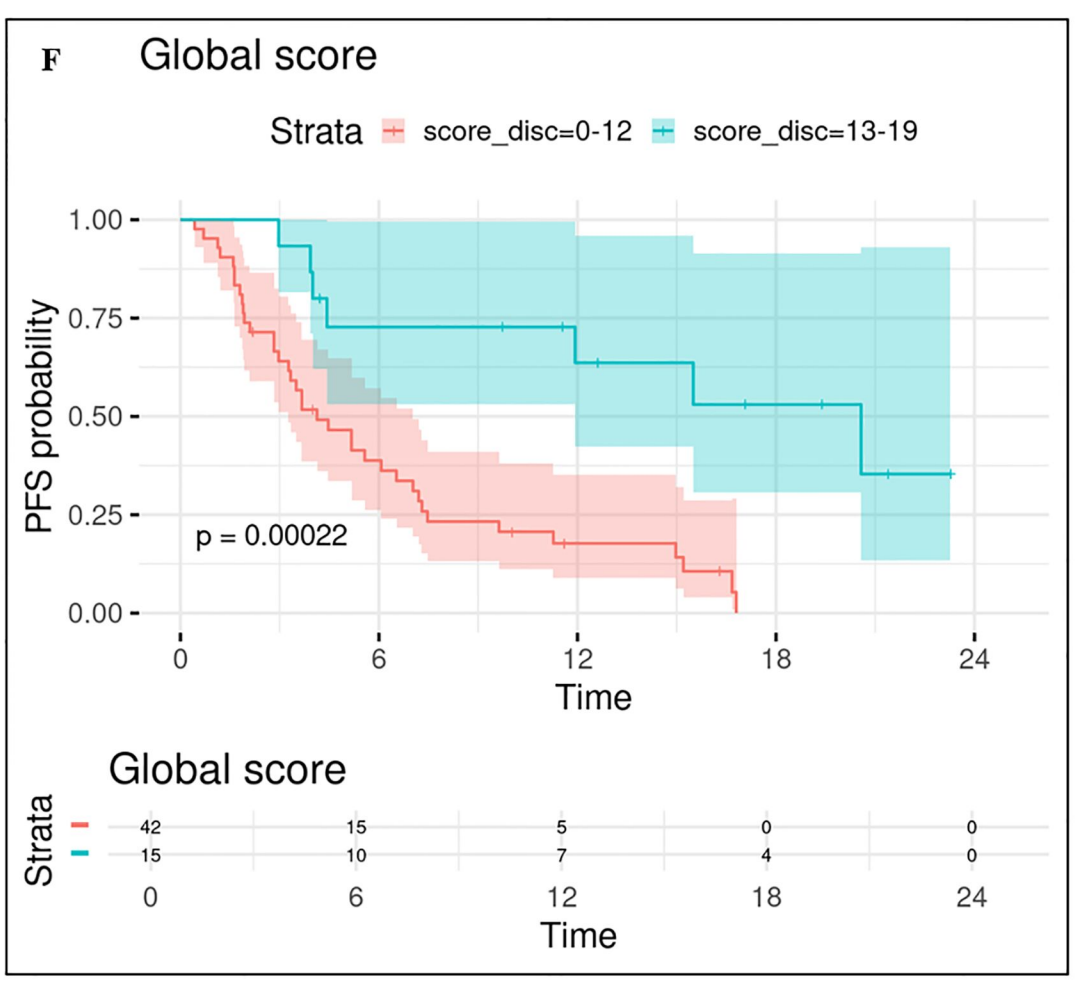

Figure 5

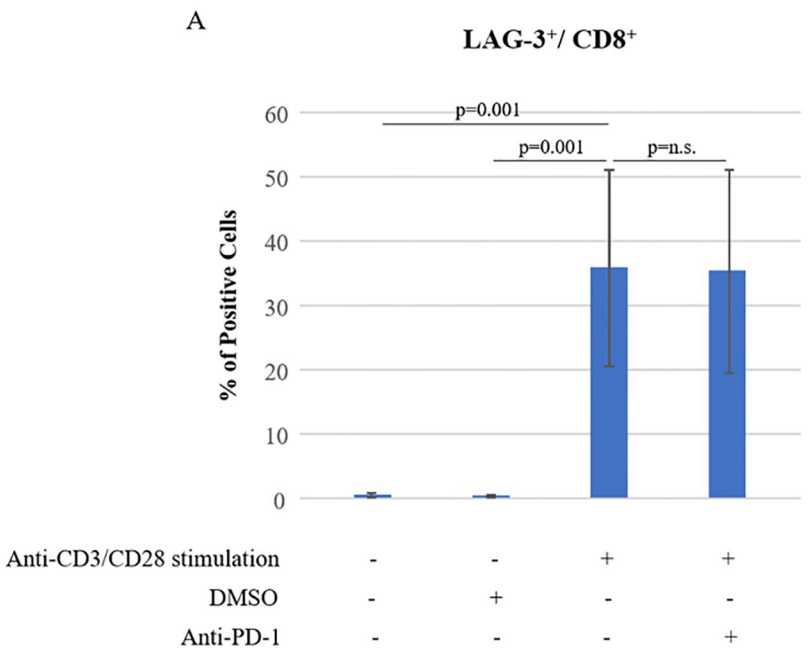

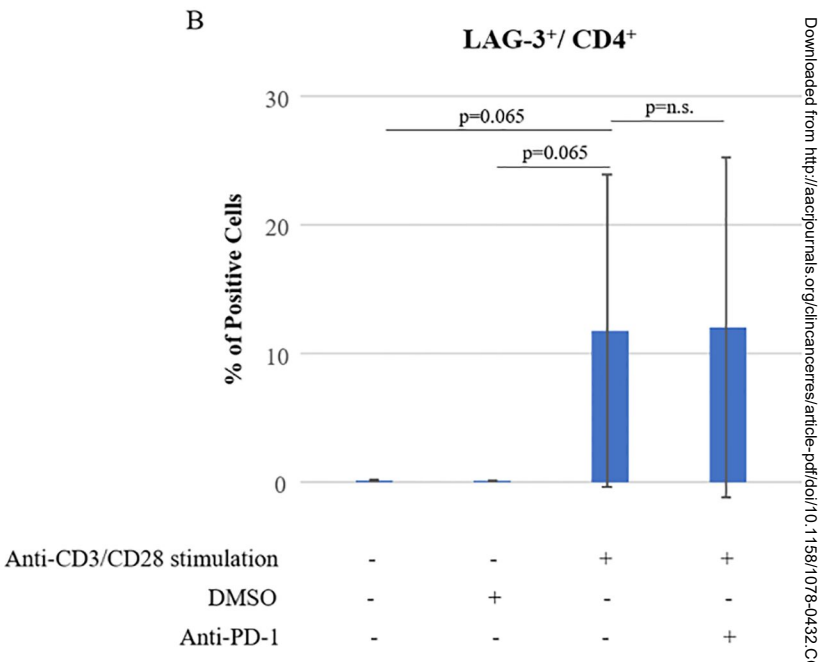

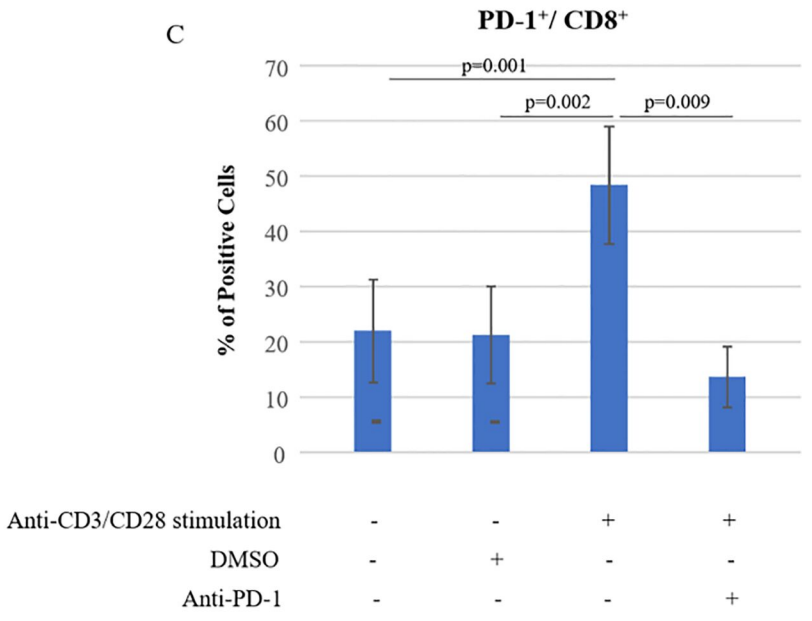

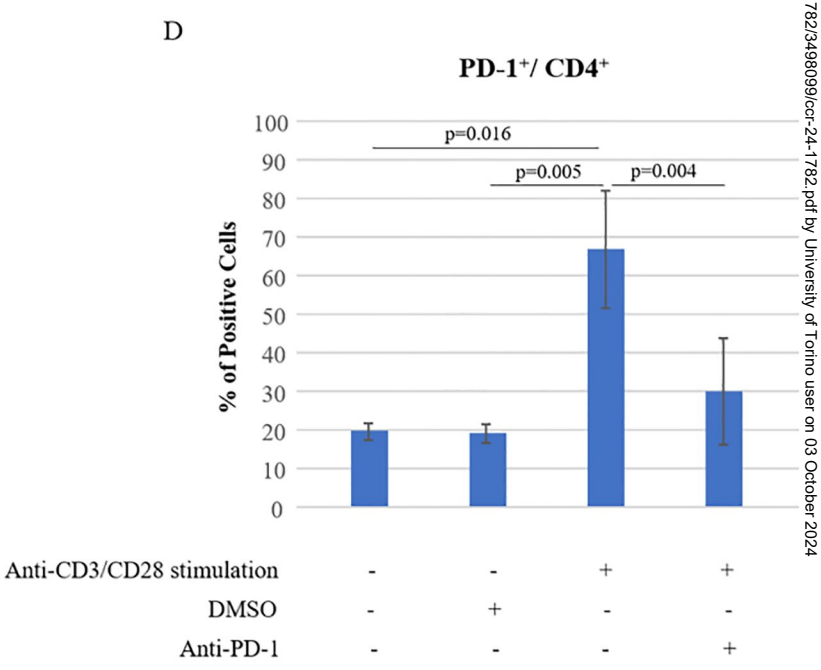

Figure 6

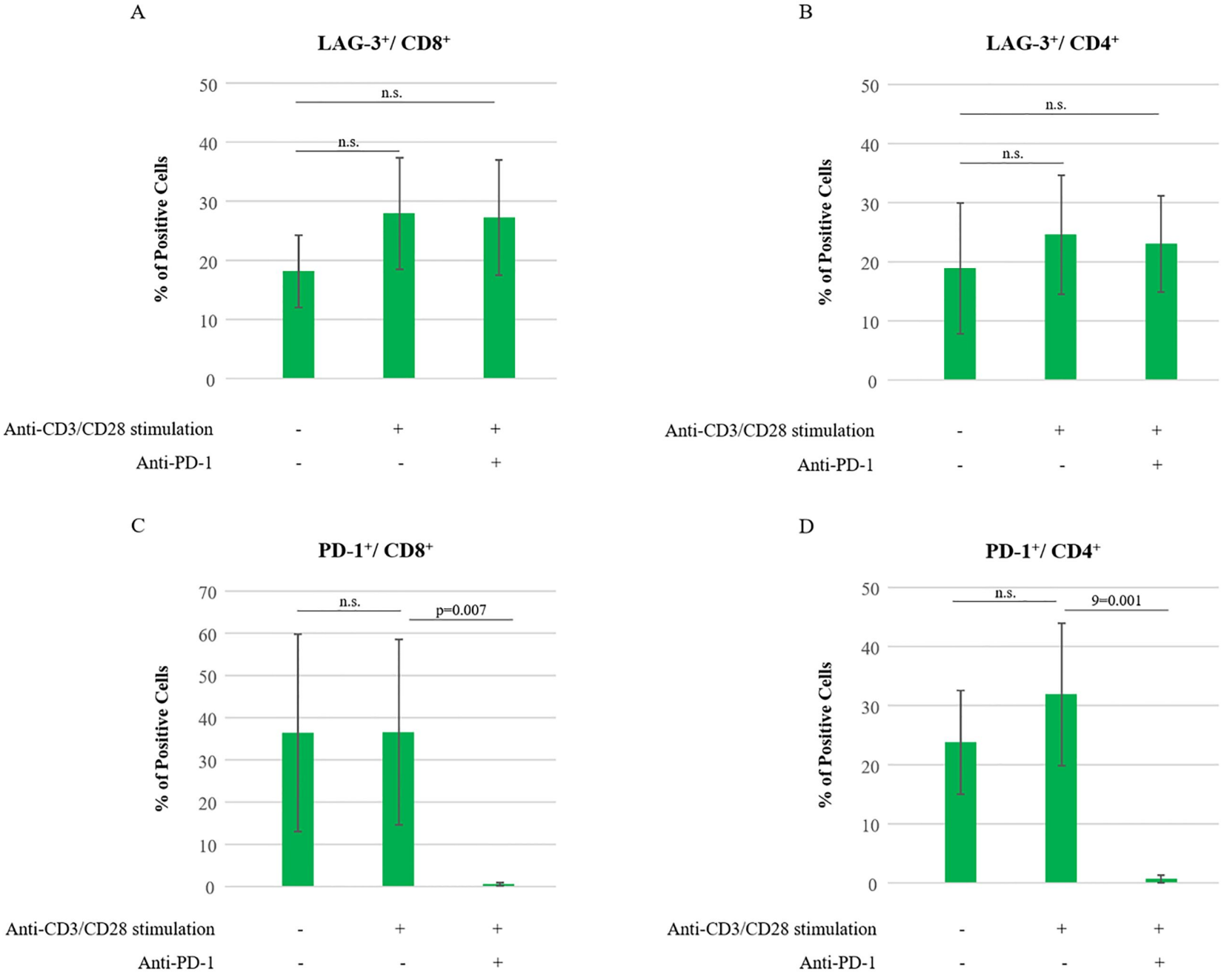

Table 1. Demographics and clinical pathological features

	(N=65)	(N=34)*	(n=35)**
Median age (range) (months)	40 (20-78)	39 (20-78)	37 (20-78)
Sex			
- Male	39 (60%)	20 (59%)	23 (66%)
- Female	26 (40%)	14 (41%)	12 (34%)
Median metastatic-free interval (range) (months)	8 (0-141)	7 (0-141)	9 (0-98)
Extension baseline:			
- Locally advanced	4 (6%)	1 (3%)	1 (3%)
- Metastatic	61 (94%)	33 (97%)	34 (97%)
ECOG at baseline			
- 0	31 (48%)	16 (48%)	18 (51%)
- 1	34 (52%)	18 (53%)	17 (49%)
Diagnosis (central):			
- Clear cell sarcoma	11 (17%)	4 (12%)	5 (14%)
- Synovial sarcoma	11 (17%)	4 (12%)	3 (9%)
- Undifferentiated pleomorphic sarcoma	10 (15%)	4 (12%)	3 (9%)
- Alveolar soft part sarcoma	7 (11%)	6 (17%)	6 (17%)
- Angiosarcoma	7 (11%)	4 (12%)	6 (17%)
- Epithelioid sarcoma	7 (11%)	5 (15%)	4 (11%)
- Solitary fibrous tumor	7 (11%)	4 (12%)	5 (14%)
- Extraskeletal myxoid chondrosarcoma	4 (6%)	3 (8%)	3 (9%)
- Epithelioid hemangioendothelioma	1 (1%)	0 (0%)	0 (0%)

*Samples used for gene expression analyses; **Samples used for soluble protein analyses.